Towards resilience of offshore wind farms

A framework and application to asset integrity management

Liu, Min; Qin, Jianjun; Lu, Da Gang; Zhang, Wei Heng; Zhu, Jiang Sheng; Faber, Michael Havbro

Published in:
Applied Energy

DOI (link to publication from Publisher):
10.1016/j.apenergy.2022.119429

Publication date:
2022

Document Version
Publisher's PDF, also known as Version of record

Applied Energy 322 (2022) 119429

Contents lists available at ScienceDirect

Applied Energy

journal homepage: www.elsevier.com/locate/apenergy

Towards resilience of offshore wind farms: A framework and application to asset integrity management

Min Liu [a,b], Jianjun Qin [c], Da-Gang Lu [a,*], Wei-Heng Zhang [a,b], Jiang-Sheng Zhu [d], Michael Havbro Faber [b,*]

[a] School of Civil Engineering, Harbin Institute of Technology, Harbin, China
[b] Department of the Built Environment, Aalborg University, Aalborg, Denmark
[c] State Key Laboratory of Ocean Engineering, Shanghai Key Laboratory for Digital Maintenance of Buildings and Infrastructure, School of Naval Architecture, Ocean and Civil Engineering, Shanghai Jiao Tong University, Shanghai, China
[d] SEWPG European Innovation Center, Arhus, Denmark

ARTICLE INFO

Keywords:
Offshore wind farm
Resilience
Decision optimization
System-of-systems
Life-cycle performance
Asset integrity management

ABSTRACT

This paper develops a general probabilistic framework for resilience modeling and analysis of offshore wind farm (OWF), and illustrates how such a framework may be implemented within the modeling techniques and tools commonly applied in the industry. Based on this framework the significance of prevailing uncertainties and the effects of different decision alternatives relevant in the context of asset integrity management (AIM) are studied and discussed. In the framework, OWFs are modeled as system-of-systems by a hierarchical model where the life-cycle performances of each system, as well as the dependencies between these systems, are represented probabilistically. The quantification of resilience is undertaken based on a scenario-based modeling of life cycle benefits and costs in which resilience failure is defined as the exhaustion of the economic capacity accumulated by the system over time. Moreover, this paper introduces resilience-informed decision-making for OWF in the context of AIM. The proposed framework is applied to the OWFs populated with NREL 5MW offshore wind turbines (OWTs). Events of typhoon-induced waves and winds are considered as the two random environmental load processes affecting the OWF's dynamic responses and for which their resilience performances are carried out. Finally, the resilience performances of the OWFs are studied and discussed for a range of decision alternatives relevant to AIM.

1. Introduction

Wind energy has emerged as a promising alternative energy source to fill the world's energy supply and demand gap. A major driver for wind energy use is the development of sustainable technologies to address some of the key issues associated with traditional fossil fuels, such as global warming, political uncertainty, and market volatility [1–5]. As is stated by the Global Wind Energy Council (GWEC), 2020 was the best year in history for the global offshore wind industry with 6.5 GW of incremental installed capacity and it is also forecasted that by 2030, the globally incremental installed offshore wind capacity will exceed 205 GW [6].

A great deal of research has been conducted concerning risk analysis and management for offshore wind energy. To support the asset integrity management (AIM) of offshore wind farms (OWFs), the input requirements (e.g. failure rates, failure costs, average repair time) are analyzed through the operational data [7–11], and probabilistic models of OWF performances are built by researchers to support decision analysis based on these inputs [12–14]. Different with onshore wind farms, OWFs are subject to met-ocean conditions leading to substantial uncertainties in their performances. Methods to estimate extreme met-ocean conditions and the associated loads are proposed to minimize the uncertainties of extreme loads [15–17]. Some of the extreme conditions like hurricanes in the USA and typhoons in Asia have big differences from the conditions in Europe, leading to the failures of wind turbines designed for European conditions observed in these regions in the past years [18]. Therefore, studies on methods and frameworks for quantifying the risk of OWFs exposed to hurricanes or typhoons have been conducted over the past few years [19–21]. The components of OWTs are vulnerable to the harsh met-ocean conditions and OWFs are far away from the shore, which makes maintenance difficult and expensive. Therefore, different O&M strategies for OWFs to reduce the direct and indirect economic losses are proposed by researchers [22–25]. To

* Corresponding authors.
E-mail addresses: ludagang@hit.edu.cn (D.-G. Lu), mfn@build.aau.dk (M.H. Faber).

https://doi.org/10.1016/j.apenergy.2022.119429
Received 9 August 2021; Received in revised form 9 May 2022; Accepted 3 June 2022
Available online 24 June 2022

quantify the economic performance of the OWF projects, the levelized cost of energy (LCoE) which aims to quantify the net present value of the cost to produce a unit of energy and the operating expenses (OPEX) are the common metrics for supporting the wind farm decisions [26]. From the perspective of AIM, the performance characteristics of wind turbines and wind farms not only depend on their physical properties, which are the usual subjects for engineering, but also on the performance of the management system and capacity of the economic system, which represent the ability of the system to provide reliable services efficiently, and sustain and recover from possible disturbances in the long term. These implies that it is crucial to adopt a performance indicator that could represent the relationship between the overall system performance and the performance of different subsystems, for which resilience that represents the ability of systems to sustain and recover from disturbance may be applied to support AIM.

Since Pimm [27] and Holling [28] introduced the fundamental ideas and insights on ecological systems resilience, significant research efforts have been devoted to the topics of the resilience of other systems [29,30]. With respect to infrastructure systems, the studies on resilience mainly focus on the formulation of resilience assessment framework especially on the definition and quantification of resilience. Bruneau et al. [31] proposed a conceptual framework for the study of resilience of infrastructures. This framework was divided into four dimensions: technical, organizational, social, and economic (TOSE), related to physical systems, the capacity of organizations, the negative consequences associated with the loss of critical services of communities and governments and the capacity to reduce economic losses respectively. Each dimension is measured by four indicators (4R's): robustness, rapidity, resourcefulness and redundancy. Zhou et al. [32] developed a framework for quantifying how aggregation of microgrids could provide significant contribution to resilience services from system-level. To facilitate the quantification of resilience, Roege et al. [33] identified a energy resilience matrix which provided a structured and comprehensive framework of metrics relevant to energy system resilience. Moslehi et al. [34] utilized a three-dimensional loss matrix to support the quantification of resilience and evaluate the cost-effective resilience enhancement strategies. Faber et al. [35,36] proposed a new approach for the modeling of resilience from a more comprehensive perspective, which accounted for in principle all possible disturbance events during the service life of the system instead of only one event in a given disturbance scenario. Apart from the definition and quantification, the other studies on resilience mainly focus on the modeling of system recovery process and resilience enhancement method. Ouyang et al. [37] divided the recovery process of infrastructure systems into three phases, namely the disaster prevention phase, the damage propagation phase and the recovery phase, and proposed the corresponding resilience enhancement strategies for each phase. Sharma et al. [38] developed a mathematical model for system recovery, by which the recovery cost is optimized. In Ref. [39], a multi-phase performance curve was applied to model the multi-energy system response and a service-based optimal energy flow model was proposed to minimize the consequences.

These existing research on resilience modeling and quantification generally focused on presenting the general idea, while the application of resilience informed AIM of OWF are not well illustrated. The following issues, which necessitate to be highlighted for AIM of OWF, are overlooked in the existing studies: (i) there are dependencies between system functionality and asset integrity management; (ii) the capacities/abilities supporting the system recovery (e.g., economic capacities, management abilities), which are critical to the resilience performance of the system, actually change overtime; and (iii) the framework that can be directly implemented with the modeling techniques and tools commonly applied in the industry is missing. The present paper develops a general probabilistic framework for OWF system representation and resilience analysis aiming for the practical implementation in the offshore wind industry. The main contributions of the present paper are summarized as follows:

(1) A hierarchical system-of-systems model is first proposed to represent the life-cycle performance of the OWF systems, in which four systems (i.e., infrastructure system, economic system, environmental system, and management system) are explicitly expressed aiming to describe the dependencies between system functionality and AIM.

(2) Resilience quantification and analysis framework is developed theoretically for OWF systems as the function of the performance of the hierarchical system-of-systems. The quantification of resilience is realized over time taking the joint actions of the four systems as the basis.

(3) It is illustrated how the proposed framework may be implemented with the modeling techniques and tools commonly applied in the industry, through the development of a comprehensive case study on the OWFs populated with NREL 5MW OWTs subject to met-ocean conditions.

This paper is organized as follows. In Section 2, a hierarchical system-of-systems model is developed to represent the life-cycle performance of the OWF system. On the basis of Section 2, Section 3 outlines an analytical framework for OWF resilience modeling and analysis, and further presents resilience-informed decision making for OWFs following the proposed framework. In Section 4, the application of the proposed framework to the OWFs subject to met-ocean conditions is illustrated together with the investigations on the definition of the decision alternatives relevant to AIM from the perspective of resilience.

2. System-of-systems representation for OWF systems

An OWF system is a typical case of hierarchical interrelated systems, i.e. a system-of-systems, where all relevant physical processes, environmental systems, geo-hazard systems, engineered objects and facilities, organizational processes, human activities as well as all decision alternatives envisaged for designing and managing the OWFs are logically interrelated. To provide decision support for AIM of OWF systems, it is crucial to establish the system representation in terms of these logically interrelated systems at various levels of detail or scale in time and space. A hierarchical model composed of the infrastructure system, economic system, environmental system, and management system is established to facilitate system modeling as well as decision analysis in the present paper, see Fig. 1. The main purpose of Fig. 1 is to provide an illustration of how OWF subsystems are hierarchically interconnected at different levels and to support the definition of the system boundary. This model is a generalized one that can be adjusted depending on the decision problems. Therefore, in the following subsections, the illustrations of the four systems shown in Fig. 1 are provided to define the system boundary and explain how systems are interrelated from a broad point of view. Then, in order to further explain the modeling of each system and how the model supports decision-making, the detailed modeling of each subsystems including the physical formulas and how can they be achieved are illustrated in Section 4 combined with the case study. For convenience, let WT_i $(i = 1, 2, \ldots, n)$ represents the i^{th} wind turbine, where n is the number of OWTs of the considered OWF; WT_{i_j} represents the j^{th}component (subsystem) of the i^{th} wind turbine $\left(i = 1, 2, \ldots, n; j = 1, 2, \ldots, n_c\right)$, where n_c is the number of considered components (subsystems) of each OWT.

2.1. Management system

In the management system, the decision-makers and stakeholders mainly consider how to manage the OWF system efficiently, ensure sufficient power generation, maximize benefits and improve resilience and sustainability performances. In addition, AIM decisions must comply with codes and standards defined by higher-level systems such as the social system and the regulatory system. These requirements will however not be addressed in detail in this paper. At the highest level in the hierarchical model, the performances of the management system will affect other systems by the consequences associated with

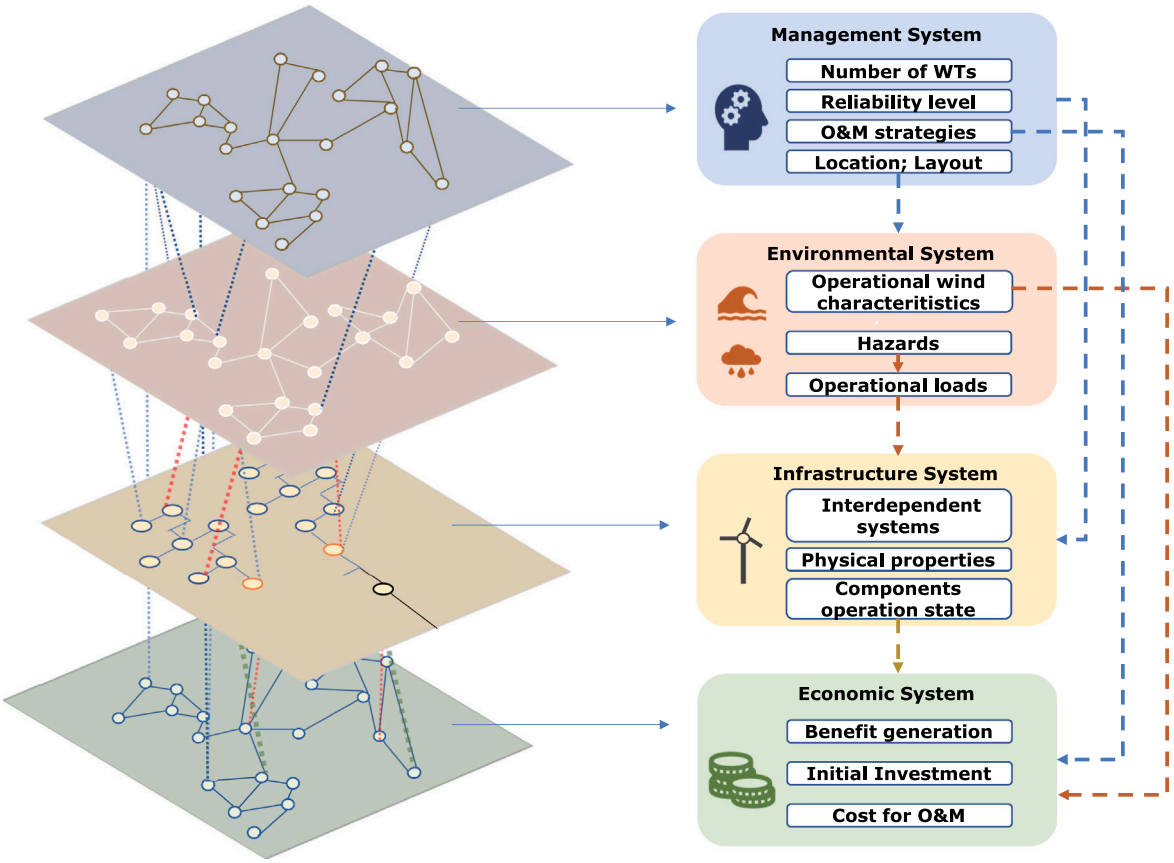

Fig. 1. Illustration of interdependent OWF systems by a hierarchical model.

AIM decisions. For instance, the design decisions on the layout may affect the energy production of the OWF; different O&M strategies may lead to different failure consequences. The decision alternatives in the management system may be divided into two categories: decision alternatives for design (e.g. layout of OWFs, types of equipment) and decision alternatives for operation management (e.g., O&M strategies). Let $\mathbf{a} = \left\{\mathbf{a}_1, \mathbf{a}_2, \mathbf{a}_3, \ldots, \mathbf{a}_{n_d}\right\}$ be a vector containing all relevant decision alternatives from the management system that may be applied for AIM, which includes but not limited to: (1) number of wind turbines (WTs) (represented by $\mathbf{a_1}$); (2) reliability level (represented by $\mathbf{a_2}$); (3) O&M strategies (represented by $\mathbf{a_3}$); (4) WT location (represented by $\mathbf{a_4}$); (5) OWF layout (represented by $\mathbf{a_5}$). The relationship between the management system and other systems will be introduced in the following sections.

2.2. Environmental system

In this paper, the environmental system not only refers to the natural environment, but also includes the operational environment in a broader sense. This section describes the environmental system in terms of three components (or sub-systems): hazards, operational loads and wind characteristics. Hazards and operational loads are the two main causes of OWT components/systems failures, while wind characteristics determine the energy production of OWT.

2.2.1. Hazards

OWFs are prone to several natural hazards such as earthquakes, extreme winds and extreme waves. In general these hazards may all individually lead to serious events such as tower collapse and broken blades [40,41]. There are two levels of dependencies between different types of potential (natural) hazards at the location of OWF which is assumed to be comprised by n WTs: The first level is the dependency between different types of hazards. For example, the typhoon induced extreme winds and extreme waves may be interrelated [16,19–21]. The second level is the dependency due to geographical proximity of two or more wind turbines. For example, there is a spatial correlation between the extreme wind speeds at different wind turbine locations. Let $\mathbf{H}_i$ be a vector containing the indicators of all relevant hazards, including the extreme winds, extreme waves, earthquakes, etc., at the location of WT_i, which depends on the location and the layout of OWFs and time t. Therefore, $\mathbf{H}_i$ may be expressed as the function of $\mathbf{a_4}$ and $\mathbf{a_5}$, and time t. More details about how to model different hazards and how to assess the performance of OWTs under multiple hazards can be found in [42–46].

2.2.2. Operational loads

In addition to failures due to extreme loads, operational loads may also cause failures of the components/systems. For example, fatigue loads caused by the actions of waves and wind would cause fatigue damage and even further lead to fatigue failures of offshore wind turbines [47,48]; corrosion can be regarded as another operational exposure or load that causes strength degradation, and the joint effect of corrosion phenomena and fatigue loads is also an significant issue which needs to be considered when analyzing the life-cycle cost [49]. There are also two levels of dependencies between the operational loads: (1) dependencies between different types of operational loads [16,50], and (2) dependencies due to the geographical proximity of wind turbines [51,52]. Let $\mathbf{L}_i$ be a vector containing all relevant operational loads, including the fatigue loads, corrosion, etc., at the location of WT_i acting on WT_i. Similarly as $\mathbf{H}_i$, $\mathbf{L}_i$ may also be expressed as the function of $\mathbf{a_4}$, $\mathbf{a_5}$ and t.

2.2.3. Operational wind characteristics

The characteristics of the wind acting on wind turbines is not only relevant for the assessment of possible evolving damages and

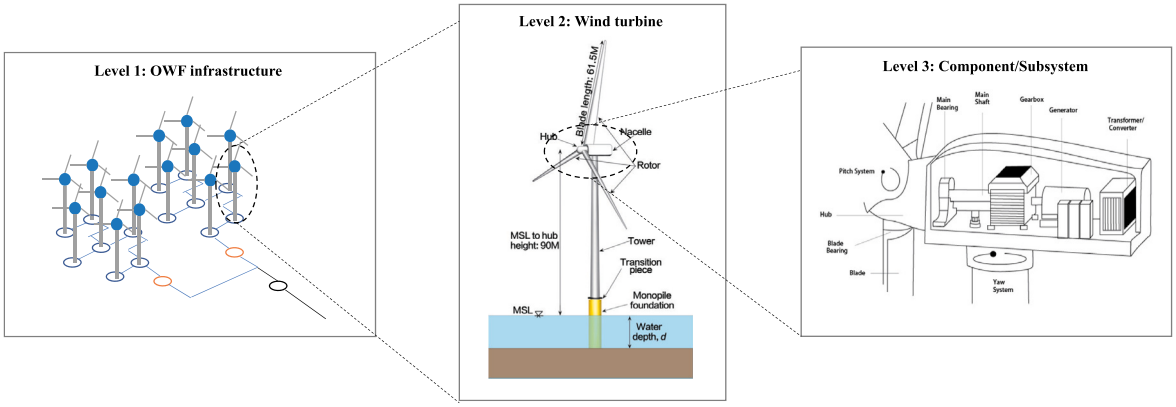

Fig. 2. System representation of OWF infrastructure system.

failures, but also comprise the source of energy. The operational wind characteristic at the location of the wind farm may significantly affect the profitability of the wind farm. For power generation of OWFs, the wind direction and wind speed are the two most important wind characteristics [53]. Normally, the wind rose divided into 8 or 12 direction sectors is used to represent the probabilistic characteristics of wind direction and wind speed, in which the wind direction is considered as a random variable characterized by the probability of occurrence for each of the sectors of the wind direction and the two-parameter Weibull probability distribution may be adopted to represent the wind speed [54–56]. Recently improved probabilistic models for the wind speed are proposed in [57,58]. The probabilistic model of the wind direction and wind speed at the location of WT_i are denoted by $\mathbf{w}_{d_i}$ and $\mathbf{w}_{s_i}$ respectively ($i = 1, 2, \ldots, n$), and represented by a vector $\mathbf{W}_i$. $\mathbf{W}_i$ also depends on the location and the layout of OWFs which represented by $\mathbf{a_4}$ and $\mathbf{a_5}$ and also time t [53,59].

2.3. Infrastructure system

The infrastructure system of an OWF system consists of different interdependent subsystems, each of which also consists of interrelated subsystems and components. This results in the fact that the performance of the OWF infrastructure system highly depends on the joint performances of all these subsystems and components. Therefore, the modeling of OWF infrastructure systems may be modeled as a three-level system, see Fig. 2. The first level is the OWF infrastructure system, where each wind turbine may be considered as a node that generates electricity and then is transformed by the transmission system. The second level is the wind turbine system, where different subsystems (e.g., energy-receiving system, energy-producing system) interact with each other to ensure that wind turbines operate according to intentions. The third level is the wind turbine subsystem, where each subsystem provides some kind of functionality with the joint work of its constituents. For example, the energy-producing system is composed of main bearing, main shaft, generator, gearbox etc.; these components work together (interact) to produce electricity. The parameters included in the vector $\mathbf{x}_{i_j}$ represent the physical properties of each component WT_{i_j}, relevant to their condition states subject to natural hazards and operational loads and the realizations of their performances (e.g., tower diameter and thickness, material yield stress, rotor diameter). Correspondingly, the vector $\mathbf{X}_i$ represents the physical properties of WT_i, which can be expressed as the function of $\mathbf{a_4}$. The performances of OWF infrastructure system not only depend on the characteristics of the system itself, but is also influenced by the environmental systems and the management systems. For example, the hazards and operational loads of environmental system may cause failures of components and even the whole system, while the maintenance strategies ($\mathbf{a_3}$) may affect the times to recovery of these components or systems. It is assumed that WT_i may attain two discrete states (failure or operation), represented by $s_i = 1$ and $s_i = 0$ respectively. The above outline shows that s_i is a function of $\mathbf{a}$, $\mathbf{X}_i(\mathbf{a}, t)$, $\mathbf{H}_i(\mathbf{a}, t)$, and $\mathbf{L}_i(\mathbf{a}, t)$.

2.4. Economic system

The performance of the economic system is influenced by the joint performances of the previously described three systems, see Fig. 1. The infrastructure system harvests wind energy to generate power which is then transported to shore and finally converted into income. The energy production of WT_i may be calculated by its power performance (included in $\mathbf{X}_i$) and the historical wind conditions $\mathbf{W}_i$. But wind turbines cannot be available all the time, and if they fail to operate i.d. ($s_i = 1$), the downtime is associated with an energy production loss and associated loss of income. The length of the downtime of WT_i highly depends on the component state s_i, and the decisions on O&M strategies ($\mathbf{a_3}$). In addition to power generation, some economic variables also have a direct influence on the economic behavior of OWFs, such as the selling price of energy and the interest rate. Of course, the economic system not only includes earnings, but also the corresponding expenses. There are some fixed expenditures such as costs of project development and wind turbine supply and installation. In addition to this, there are many expenses that are subject to uncertainty, such as O&M costs, which are influenced by the components state s_i and the decisions on O&M strategies. For OWFs, the O&M costs are much higher compared to onshore ones due to the harsh environmental conditions leading to higher failure rates and longer repair time. Section 3.2 holds further details associated with the modeling of maintenance cost and downtime.

3. Resilience analysis and decision support framework for OWF systems

This section starts with an introduction to the resilience modeling and quantification method. Later, illustrations are provided of the modeling approaches for OWF system failures and the associated consequences, to facilitate resilience analysis. Finally, Section 3.3 explains how the proposed resilience modeling approach can be applied to support decision-making for OWF systems in the context of AIM.

3.1. Resilience modeling and quantification

This paper aims to develop the probabilistic resilience model for the AIM of OWF systems. The idea is illustrated in Fig. 3. There are two different realizations of the evolution of benefit generation (per unit time), economic reserve as the function of benefit generation (per unit time), and the accumulated economic capacity: one realization without resilience failure and one with resilience failure. For illustration purposes, the evolution of benefit generation shown in Fig. 3

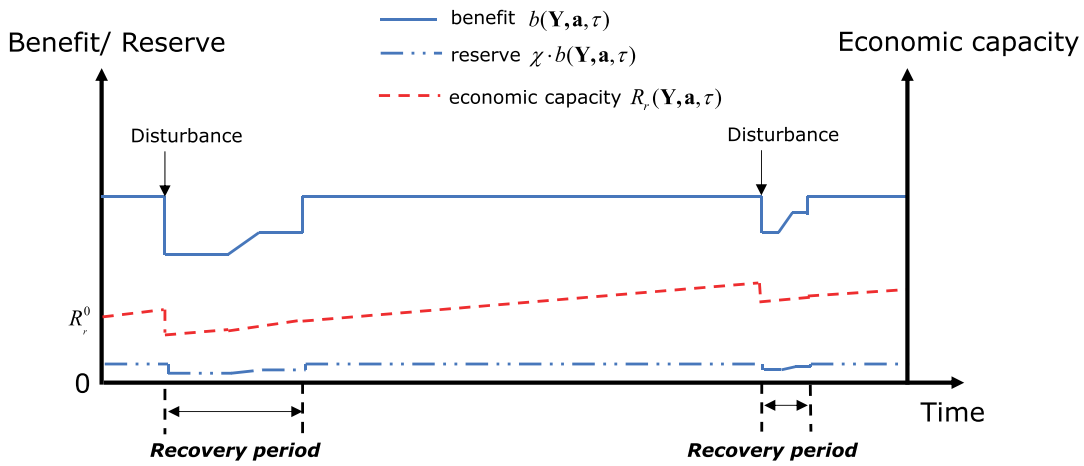

(a) A scenario with no resilience failure

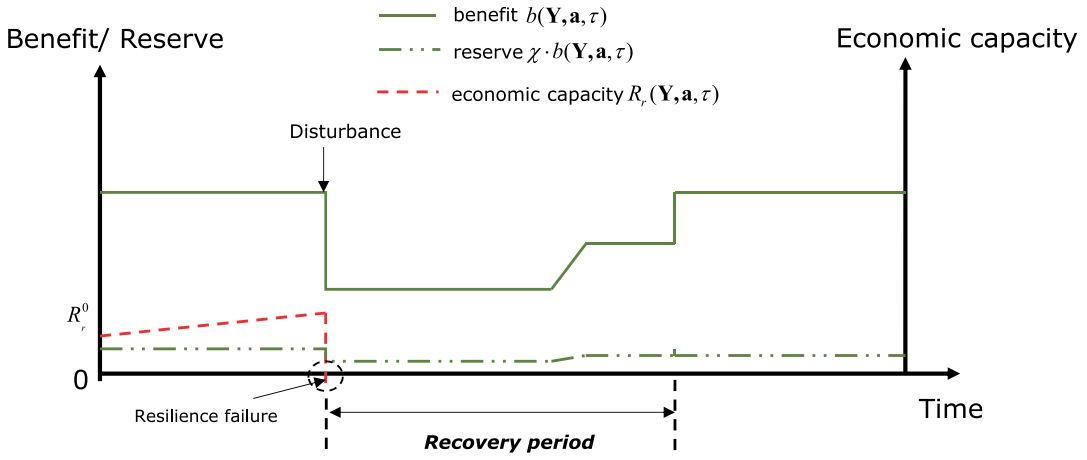

(b) A scenario with resilience failure

Fig. 3. Illustration of resilience model in terms of the evolution of benefit generation and the corresponding evolution of accumulated reserves with time, together with the time varying demands caused by disturbances.
Source: Adapted from Faber et al. [35].

is assumed to be constant over time in case that the whole farm is under normal operation state, only WT failures caused by disturbance events will decrease the benefit generation during the recovery period. However, in reality, the benefit generation fluctuates with the time-varying parameters such as wind speed and energy selling price under normal operation state. As illustrated in Fig. 3, the benefit generation can be expressed as:

$$b(\mathbf{Y},\mathbf{a},\tau) = ep(\mathbf{Y},\mathbf{a},\tau) \times p_{\mathrm{E}} \tag{1}$$

where P_{E} is the selling price of energy; $ep(\mathbf{Y},\mathbf{a},\tau)$ is the power production function of the wind farm which is the function of time τ; $\mathbf{Y}$ is a vector contains all the random variables which are introduced in Section 2, including $\mathbf{X}_i$, $\mathbf{H}_i$, $\mathbf{L}_i$, $\mathbf{W}_i$, etc.; $\mathbf{a}$ is a vector contains all decision alternatives from the management system.

The economic capacity with respect to resilience $R_r(t)$ is obtained by accumulating a fixed percentage of the benefit $\chi \cdot b(\mathbf{Y},\mathbf{a},\tau)$ as economic reserve over time to meet the economic demand due to system failures. As illustrated in Fig. 3, the economic capacity concerning resilience at time t may be expressed as the accumulation of the evolution of the reserves:

$$R_r(\mathbf{Y},\mathbf{a},t,\chi) = R_r^0 + \int_0^t \frac{\chi b(\mathbf{Y},\mathbf{a},\tau)}{(1+r)^{\tau}} d\tau \tag{2}$$

where R_{r}^0 represents the startup economic capacity which depends on the decision on this value (e.g. some percentage of the total benefit generated in the whole service life); χ represents the saving percentage; r is known as the interest rate determined by the financial strategy. It is important to note that χ here represented by a separate variable is to illustrate how the economic capacity is acquired, but χ is also a decision alternative which is represented by $\mathbf{a}$. When a disturbance event causes system damage or failure, the system economic capacity will be reduced by the cost for system recovery, which is defined as the economic demand.

It is assumed that $\mathbf{t}_{\mathrm{F}}(\mathbf{Y},\mathbf{a})$ represents the time domain when disturbance events happened during the OWF service life. The economic demand at time t may be expressed as:

$$S_{\mathrm{r}}(\mathbf{Y},\mathbf{a},t) = \sum_{\tau \in \{\mathbf{t}_{\mathbf{F}} \cap (0,t)\}} \frac{C(\mathbf{Y},\mathbf{a},\tau)}{(1+r)^{\tau}} \tag{3}$$

where $C(\mathbf{Y},\mathbf{a},\tau)$ represents the cost for recovery after the failure event at time τ; $\mathbf{t}_{\mathbf{F}} \cap (0,t)$ represents the time domain when disturbance events happened within the time period $(0,t)$.

System resilience failure is then defined as the exhaustion of the system economic capacity (see Fig. 3(b)). The event of resilience failure at time t is defined by the following limit state function:

$$g_{\mathrm{RF}}(\mathbf{Y},\mathbf{a},\chi,t) = R_{\mathrm{r}}(\mathbf{Y},\mathbf{a},t,\chi) - S_{\mathrm{r}}(\mathbf{Y},\mathbf{a},t) \tag{4}$$

For a given time period (t_1,t_2)(e.g., one year), the probability of resilience failure happened within the time period can be calculated by

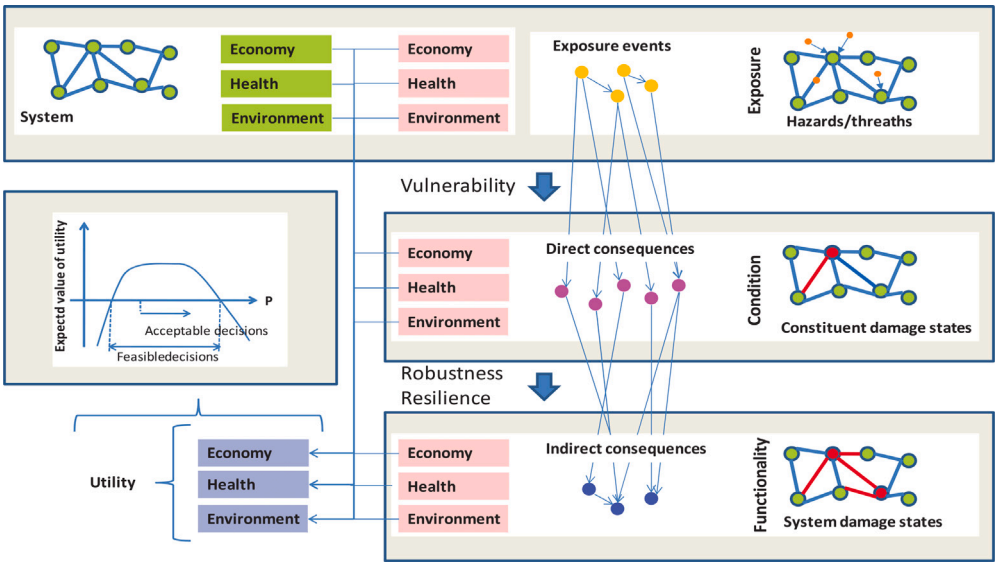

Fig. 4. Generic framework for decision analysis of systems [36].

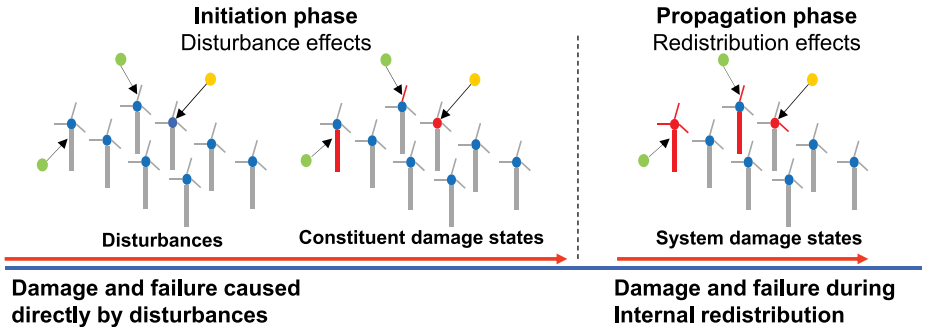

Fig. 5. Illustration of the two-phase scenario based failure propagation model.

the following equation:

$$P_{\mathrm{RF}}(\mathbf{a}, \chi, (t_1, t_2)) = P\left\{ \{\min\{g_{\mathrm{RF}}(\mathbf{Y}(\tau), \mathbf{a}, \tau) | \tau \in (0, t_1)\} > 0\} \cap \{\min\{g_{\mathrm{RF}}(\mathbf{Y}(\tau), \mathbf{a}, \tau) | \tau \in (t_1, t_2)\} < 0\} \right\} \quad (5)$$

3.2. Modeling of failures and consequences

The modeling of failure events and the failure consequences are crucial for resilience analysis. The system modeling approach suggested by the JCSS [60] is utilized to model the scenarios of failure events and the corresponding consequences, see Fig. 4. In the following two sections, the modeling of system failures and failure consequences are introduced respectively.

3.2.1. Modeling of system failures

The failure of a system may be modeled as a two-phase phenomenon: the initiation phase and the propagation phase, see Fig. 5. In the initiation phase, a disturbance event causes damages or failures of some constituents. Following these events in the initiation phase, the demands of the constituents of the system are redistributed until both internal and external demands are in equilibrium with the capacity of the system or until the system totally fails. This process may occur in a sequence of failures and subsequent redistribution — denoted as cascading failure scenarios. The modeling methods of the two phases of failures will be introduced in the following two parts respectively.

Initial phase of system failure. The modeling methods of the initial phase are divided into two groups: The first group is the modeling methods for structural components (e.g., blades, foundation, tower) and some mechanical components (e.g., shaft, gearbox) [22]. For these components, limit state functions (LSFs) can be formulated to model different failure modes (e.g., local or global buckling failure of towers, fatigue failure of blades or details in substructure, foundation failure by sliding [61]). LSFs of WT_{i_j} are denoted by a vector $\mathbf{F}_{i_j} = (F_{i_j}^1, F_{i_j}^2, \ldots, F_{i_j}^{n_{i_j}})$, where n_{i_j} is the number of LSFs of WT_{i_j}. For each component, if any LSF $F_{i_j}^k \left(k = 1, 2, \ldots, n_{i_j}\right)$ is less than zero, there are some failure events. Generally, each $\mathbf{F}_{i_j}$ is the function of $\mathbf{x}_{i_j}(\mathbf{a}, t)$, $\mathbf{H}_i(\mathbf{a}, t)$, $\mathbf{L}_i(\mathbf{a}, t)$. More details about the identification of important failure modes of these components and the stochastic modeling of the uncertain parameters can be found from [61,62]. The second group is the modeling methods for electrical components and some mechanical components. Damage states in these components are rather difficult to detect by means of inspections, and the failures generally occur suddenly without any precursor. Classical reliability analysis methods can be used to model these components [9,63]. The variation of the failure rate with time may be expressed by the bathtub curve, see Fig. 6. Usually, the power law process (PLP) is used in the reliability analysis of these components [63]. The failure rates of the three phases in the bathtub curve may be described by the intensity function $\lambda(t)$:

$$\lambda(t) = \frac{\beta}{\theta}\left(\frac{t}{\theta}\right)^{\beta-1} \quad (6)$$

where β is a shape parameter describing the change of intensity function; θ is a scale parameter and $\theta > 0$ for $t \geq 0$. Three phases in Fig. 6

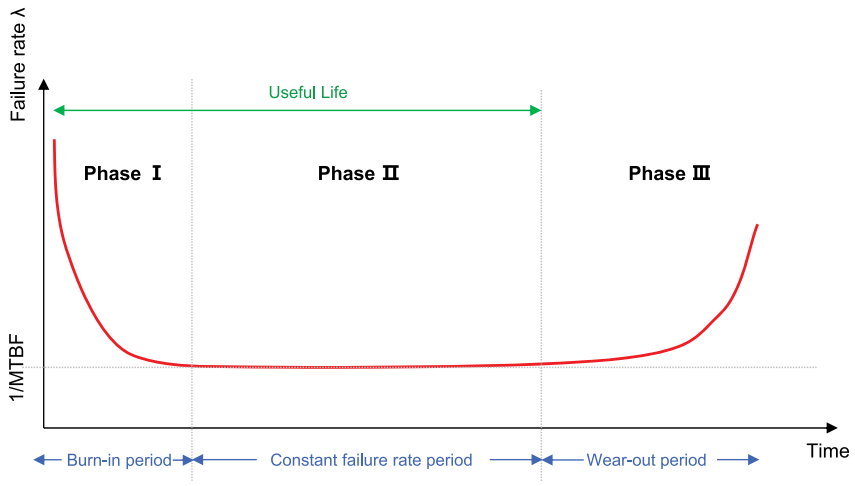

Fig. 6. Bathtub curve of a OWT component [22].

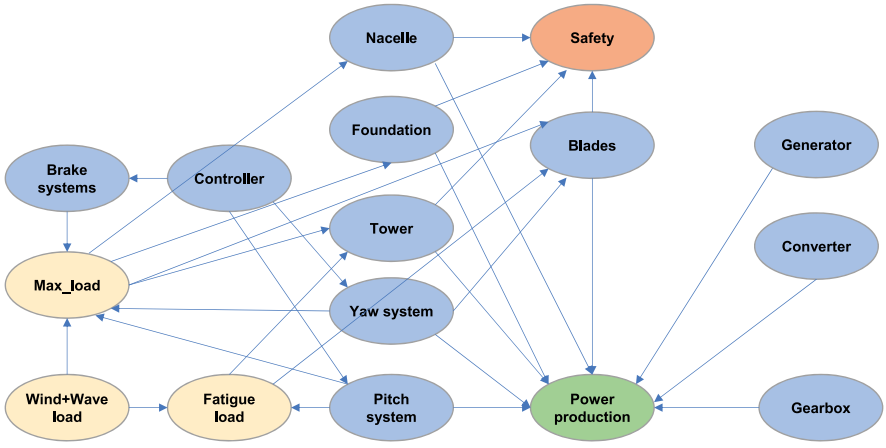

Fig. 7. Illustration of the interdependence and joint performance of all sub-systems/components of OWT.

correspond to $\beta < 1$, $\beta = 1$, $\beta > 1$ respectively. When $\beta = 1$, Eq. (6)becomes a constant and the process is a homogeneous Poisson process (HPP). Thus θ becomes the mean time between failures (MTBF), which can be estimated from databases on operational performance [9,63].

Propagation phase of system failure. To model system failures in the propagation phase, it is important to identify the different failure modes of the wind turbine system and their inter-dependencies. There are different methods such as Fault Tree Analysis (FTA) and Failure Mode and Effect Analysis (FMEA) [45,64] that can be applied to identify the failure modes of OWT systems. But recently, according to [65], the Monte Carlo simulation combined with bid data techniques are applied to identify the scenarios which contribute to system failures and the corresponding consequences from a more quantitative perspective. Based on the failure mode analysis, the dependencies between different components can be modeled. Fig. 7 illustrates the interdependence and joint performance of some of the components/sub-systems of OWTs. From Fig. 7 it is seen that the performance of structural components of the OWTs (e.g., blades and towers) may be adversely affected by malfunctions and failures of the pitch system and the yaw system. The conditional failure probabilities of components and sub-systems of OWT's can in principle be obtained through databases with operational failures, however only if relevant data are available, otherwise probabilistic mechanics analyses are more adequate.

3.2.2. Modeling of failure consequences

The consequences following failures of constituents, sub-systems and systems are differentiated into two principal categories, namely direct and indirect (or follow-up) consequences, see Fig. 4. Direct consequences are most often associated with individual constituent failure whereas indirect consequences are associated with loss of system functionalities and services caused by individual failures as well as combinations of constituent failures. For OWF systems, direct consequences may be associated with the economic cost arising during the period of wind farm recovery (i.e., the economic demand). Fig. 8 shows the possible sources of recovery cost, from which it is seen that the recovery cost after a failure event may be calculated by:

$$C = C_{\mathrm{w}} + C_{\mathrm{trans}} + C_{\mathrm{material}} \tag{7}$$

where C_{w} is the total labour cost, which generally depends on the time spent during the maintenance phase, the testing phase and the choice of maintenance team [9]; C_{trans} is the transportation cost, which depends on the type of the failed constituents and the choice of the transportation [22]; C_{material} is the cost for materials and/or equipment, which depends on the type of the failed constituents. If a failure event occurs, the failed turbine does not produce power during the downtime, the consequences of which may be considered to be indirect. Fig. 8 illustrates the possible sources of uncertainties that may affect the downtime (mean time to recover (MTTR)), and indicates that there are three main phases of recovery: preparation phase, maintenance phase, and testing phase. From Fig. 8 it is seen that except for the performance of the OWF itself, the decisions of the management system and the environmental conditions in general also significantly influence the downtime. The downtime after a failure event may be calculated by:

$$T = T_{\mathrm{pre}} + T_{\mathrm{rep}} + T_{\mathrm{test}} \tag{8}$$

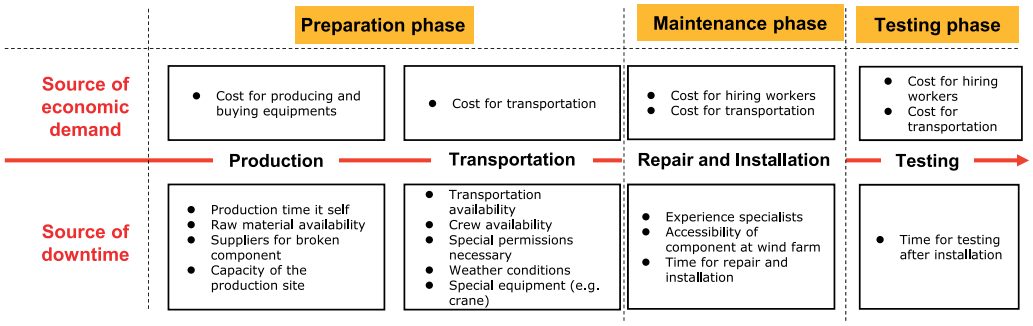

Fig. 8. Illustration of possible sources of downtime and economic demands during the period of recovery [22].

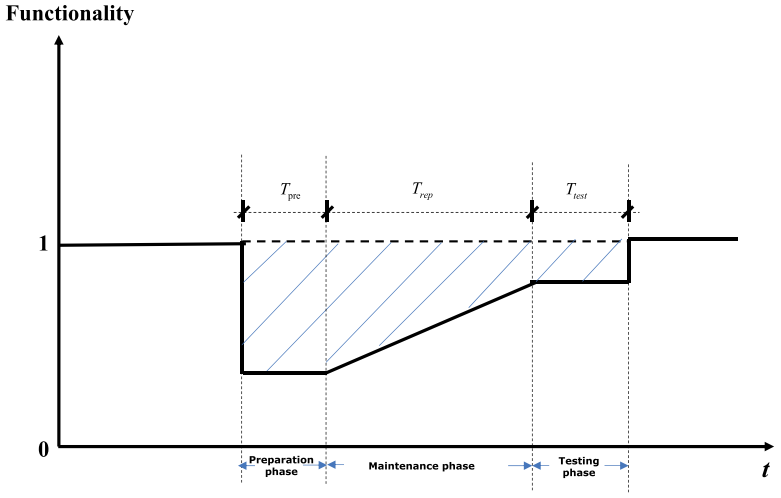

Fig. 9. Illustration of the functionality recovery of an OWF system over time after one disturbance.

where T_{pre} is the duration of the preparation phase, including the time for ordering the repair parts, briefing the technicians and preparing the helicopter/boat for the transport; for OWFs, the waiting time for the transportation will be longer due to potentially bad weather conditions; T_{rep} is the duration of the maintenance phase, which strongly depends on the number of and the types of the failed components; T_{test} represents the duration of the testing phase; for example, if the tower collapses, it will take several months to test the wind turbine after completing the installation of a new tower. The indirect consequences also depend on the functionality recovery of the systems. Fig. 9 illustrates the functionality recovery of OWF systems after a disturbance. The functionality of the system remains the same until the end of the preparation phase, then the functionality recovers after the maintenance work has been carried out. Sometimes the system's functionality is not fully recovered during the repair phase because there are components that require a long test time. After the testing phase, the OWF systems will finally recover to the original state.

It is thus a central and critical issue to be able to identify the scenarios relevant and significant with respect to the generation of consequences. To efficiently identify the individual scenarios, joint consideration of their probabilities and consequences is necessary. The assessment of their probabilities typically necessitates probabilistic analysis of unions of intersections of failure events—with due account for dependencies between these. Moreover, it should be highlighted that in practical engineering applications some of the possible scenarios may be irrelevant or physically impossible and must be excluded in the modeling, where Monte Carlo Simulation may be utilized as basis for the identification as suggested in [65].

3.3. Resilience-informed decision-making for OWF systems in the context of AIM

As illustrated in Section 3.1, the probability of resilience failure P_{RF} is the function of decision alternative **a**, see Eq. (5). Therefore, resilience modeling facilitates the decision-making for OWF by assessing P_{RF} for all possible decision alternatives. The formulation of decision problems depends to a large extent on the preferences of decision-makers. Different decision makers or stakeholders will have different preferences with respect to decision alternatives. In this section, resilience-informed decision-making regarding two different aspects will be illustrated. If the maximum acceptable probability of resilience failure is the only constraint, the acceptable decision alternatives can be identified by comparing P_{RF} of all decision alternatives with the maximum acceptable P_{RF}^{A}:

$$\text{Identify} \quad \mathbf{a}$$
$$\text{s.t.} \quad P_{RF}(a) \leq P_{RF}^{A}, \tag{9}$$

Fig. 10 illustrates the difference between two different choices of χ (the percentage of benefit (income) saving that is accumulated as system economic capacity to support the cost of system recovery) in conducting decision alternative identification, where $\chi_2 > \chi_1$. It is observed that the decision maker may adjust the range of acceptable decisions by choosing different χ. If a lower value of χ is chosen, a smaller range of acceptable decisions is obtained. Conversely, if a larger value of χ is chosen, a larger acceptable decision interval will be obtained. This indicates that from the perspective of the decision maker, an appropriately high proportion of economic reserve may increase the flexibility of decision-making. Of course, an excessively high value of χ

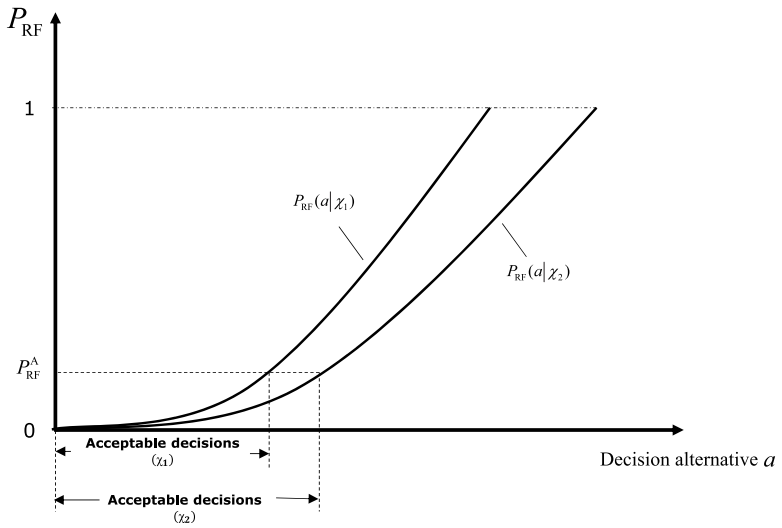

Fig. 10. Principal illustration of the identification of acceptable decisions with two different χ.

is also undesirable, but the optimization of χ is beyond the scope of this paper. However, in many cases, resilience is not the only requirement. The decision-making process is also constrained by other factors. In the following, the identification of acceptable decision alternatives under the P_{RF} and LCoE constraints will be illustrated. For OWF owners, LCoE is a main competitive indicator, which is a measure of the average net present cost of electricity generation for a generating plant during its lifetime [26]. The LCoE for a wind farm can be calculated by [66]:

$$LCoE = \frac{CAPEX \times CRF + OPEX}{AEP_{\text{potential}} - AEP_{\text{Loss}}} \tag{10}$$

where *CAPEX* is the initial Capital Expenditure; *CRF* is Capital Recovery Factor; *OPEX* is the average yearly Operational Expenditure; $AEP_{\text{potential}}$ is the average potential Annual Energy Production (AEP) of the wind farm in Watt hour (Wh); AEP_{Loss} is the average lost AEP of the wind farm due to unavailability of wind turbines or electrical infrastructure in Watt hour (Wh). Fig. 11 shows the principal illustration of the identification of acceptable decisions constrained by P_{RF} and *LCoE*. As shown in Fig. 11, the acceptable decision alternatives can be identified by assessing P_{RF} and *LCoE* for all possible decision alternatives and comparing with the maximum acceptable probability of resilience failure P_{RF}^{A} and the maximum acceptable $LCoE^{A}$:

$$\begin{aligned} &\text{Identify} \quad \mathbf{a} \\ &\quad \text{s.t.} \quad P_{RF}(a) \le P_{RF}^{A}, \\ &\qquad\quad LCoE(a) \le LCoE^{A}, \end{aligned} \tag{11}$$

Decisions that may be made to reduce the P_{RF} of an OWF will not necessarily reduce *LCoE*, see Fig. 11. For example, the decisions that require high initial capital expenditure (e.g., more expensive wind turbines) and maintenance cost (e.g., larger maintenance team) may reduce the *LCoE*. This means that the impact on *LCoE* needs to be considered when making resilience decisions.

4. Case study

In this section, the proposed resilience framework is applied and the relationships of resilience with different decision alternatives are investigated. Following Section 2, a brief introduction of the system-of-systems representation for the example OWF is given in Section 4.1. Then, based on the proposed resilience analysis and decision support framework outlined in Section 3, the modeling of system failures and failure consequence of the utilized examples are illustrated in Section 4.2. Finally, the sensitivity analysis of the example OWFs resilience subject to different decision alternatives is shown in Section 4.3.

4.1. System-of-systems representation

4.1.1. Management system

To investigate the impact of different decisions on the resilience of OWFs, four categories of decision alternatives are considered, which may be expressed as:

$$\mathbf{a} = \{\mathbf{a}_1, \mathbf{a}_2, \mathbf{a}_3, \mathbf{a}_4\} \tag{12}$$

where

- $\mathbf{a_1} = \{level1, level2, level3\}$ represents the decisions on the level of target design reliability of mechanical and electrical components, thus the failure rates of the components of the three reliability level are different, see Section 4.2.2;
- $\mathbf{a_2} = \{high, low\}$ represents the decisions on the level of preparedness, which represents the efficiency of the repair work (i.e., high preparedness means shorter preparation and repair times), see Section 4.2.4;
- $\mathbf{a_3} = \{5, 10, 15\}$ represents the decisions on the number of WTs of the OWF (three sizes of OWFs are considered in the present paper, which contains 5,10,15 wind turbines respectively);
- $\mathbf{a_4} = \{0.02, 0.04, \ldots, 0.3\}$ represents the decisions on the percentage χ of the income generated by OWFs accumulated as economic capacity.

4.1.2. Environmental system

The considered OWFs are assumed to be located at Zhanjiang, a coastal city in southeastern China, where typhoons comprise a major hazard to the OWFs. It is assumed that typhoon events occur only once a year at a random time in either July, August or September. OWTs affected by typhoons are loaded by at least two random environmental processes: turbulent winds and irregular waves [20]. The 10-minutes hub-height mean wind speed V_{hub} and the significant wave height H_S are chosen as intensity measures of these two random environmental processes. The probabilistic model of the annual extreme V_{hub} can be transformed from the annual extreme 10-minutes 10m-height mean wind speed V_{10} by the near-neutral power-law wind profile model [67]:

$$U(h) = U_H\left(\frac{h}{H}\right)^{\alpha} \tag{13}$$

where U_H is the reference wind speed at the reference height of H; h is the vertical height above the ground or the sea surface and α is the Hellmann exponent which is determined by the atmospheric stability, the mean wind speed and the surface roughness [68]; The American

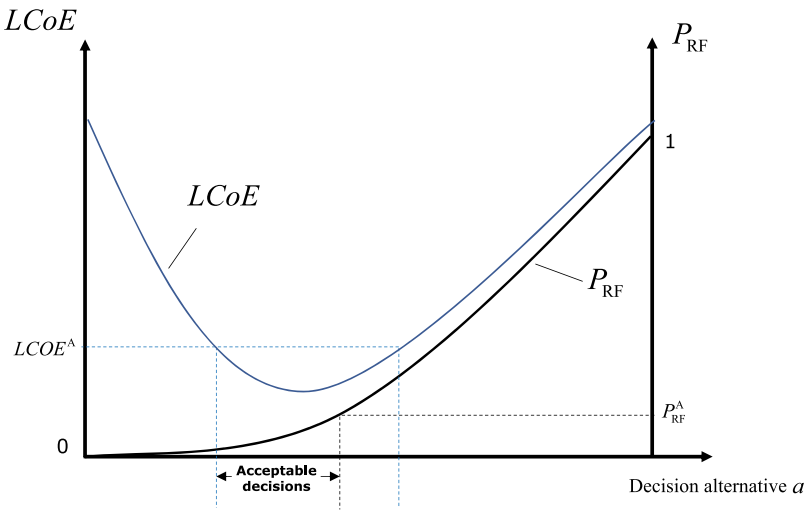

Fig. 11. Principal illustration of the identification of acceptable decisions.

Table 1
Probabilistic model of V_{10}.

City	Distribution				
	Weibull			Gumbel	
	γ	η	β	u	α
Haikou	5.95	12.33	1.62	13.86	0.18
Zhanjiang	5.634	12.04	1.65	/	/
Hongkong	5.86	12.54	1.57	13.86	0.18
Shenzhen	5.74	12.29	1.59	13.57	0.18
Guangzhou	5.73	11.70	1.59	13.19	0.18

Table 2
Main physical properties of the considered wind turbine.

Parameter	Value
Rating	5 MW
Rotor Orientation,Configuration	Upwind,3 Blades
Rotor, Hub Diameter	126 m, 3 m
Hub Height	90 m
Cut-In, Rated, Cut-Out Wind Speed	3 m/s, 11.4 m/s, 25 m/s
Mass of the rotor-nacelle assembly	350,000 kg
Tower diameter bottom, top	6387 m
Tower wall thickness bottom, top	3525 mm
Monopile diameter	6 m
Monopile wall thickness	60 mm

Bureau of Shipping (ABS) [67] recommends to choose this parameter as 0.11 when calculating wind profiles under extreme conditions (e.g., the typhoon boundary layer). According to this model, V_{hub} can be calculated as:

$$V_{hub} = V_{10}(\frac{90}{10})^{0.11} \tag{14}$$

The probabilistic model of V_{10} is taken from the model developed by Xiao [42], see Table 1. The three-parameter Weibull distribution is chosen to model V_{10}. The JONSWAP fetch limited growth relationship [16] is used to estimate the H_S conditioned on V_{10}:

$$Hs = \frac{0.0016 C_f V_{10}{}^2 (\frac{gf}{V_{10}{}^2})^{0.5}}{g} \tag{15}$$

where f represents the fetch length and is assumed to be 300 km, g is the acceleration of gravity and C_f is a depth correction factor for water depth, which accounts for the biases when applied in shallow water [19]:

$$C_f = -0.000117d^2 + 0.0197d + 0.4 \tag{16}$$

where d is the water depth, here assumed equal to 20 m. The peak spectral period (T_p) is assumed given conditional on H_s following the conditions specified by IEC-61400-3 [69]:

$$T_p = 11.7\sqrt{\frac{H_s}{g}} \tag{17}$$

4.1.3. Infrastructure system

The OWTs are assumed to be designed in accordance with the NREL 5MW OWT, with a monopile foundation [70], as shown in Fig. 12. The main properties of the considered OWTs are shown in Table 2. The design lifetime of the OWTs is assumed to be 25 years. The different OWFs (with 5, 10, and 15 OWTs) are investigated with the objective to assess the influence of the number of wind turbines on the OWF resilience performance.

4.1.4. Economic system

The capacity of the economic system is established by accumulating the income (benefits) achieved by selling electricity. The energy production of WT_i within the kth month is assumed to be:

$$EP_i(k) = EP_N(k) \times \frac{T_o(k)}{T_k} \tag{18}$$

where $EP_N(k)$ represents the energy production within the kth month of WT_i when no failures occur, see Table 3; $T_o(k)$ represents the duration of normal operation in the kth month; T_k represents the duration of the kth month. Then the benefits earned by WT_i within the kth month can be calculated by:

$$B_i(j) = \frac{EP_i(k) p_E}{(1+r)^{[\frac{j}{12}]}} \tag{19}$$

where p_E is the selling price of electricity, r is the interest rate, which is taken from Table 3. In this example, the energy production of each month listed in Table 3 is taken from the monitoring data of a 5MW OWT provided by SEWPG, and the power generation for those months without failure time is selected. For simplification, the uncertainties of power generation of wind turbines and the wake effect which could lead to the difference in the power generation of each wind turbine are not considered in the present example. The demand of the economic system is considered as the maintenance (repair) costs incurred after failures in the present research. However, the economic system established here is incompleted, only the energy loss and the maintenance costs caused by failures of the wind turbines are investigated, without considering the initial investment of the OWFs, the regular maintenance costs, etc.

Table 3
Parameters related with the capacity model of economic system.

Month	Energy production (unit:kWh)
Jan.	1584.464
Feb.	776.264
Mar.	1543.08
Apr.	901.04
May.	696.128
Jun.	659.28
Jul.	913.88
Aug.	609.92
Sept.	1019.296
Oct.	1286.4
Nov.	1035.824
Dec.	1035.824
Other parameter	Value
Price of electricity p_E (USD/kWh)	0.11
Interest rate r	0.05

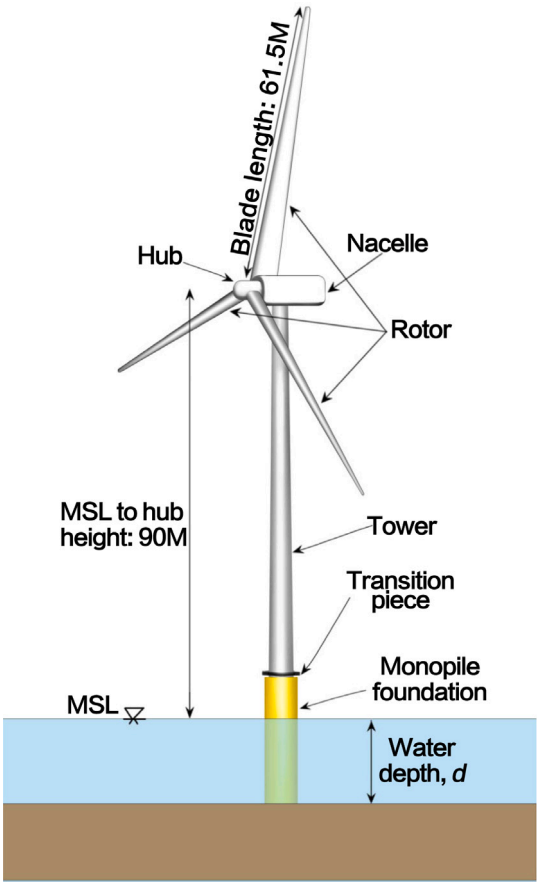

Fig. 12. NREL 5MW OWT with a monopile foundation.

4.2. System failures and failure consequence modeling

4.2.1. Modeling of structural components failures

The main failure modes of the tower and blades are fatigue failures, structural damages due to extreme winds and waves, etc., for which the representation of failure events is provided in Section 3. Only the structural failures caused by extreme winds and waves are considered in the present paper. The simulations of structural dynamic responses under the action of typhoons are carried out using FAST 8, an aero-hydro-servo-elastic simulator developed by NREL [71]. In the present paper, a database containing environmental loads and their corresponding structural failure probabilities is created. 95 combinations of $(V_{\mathrm{hub}}, H_{\mathrm{s}})$ are chosen, where the hub-height wind speed V_{hub} is assumed to change from 5 m/s – 100 m/s and then the corresponding reliability for these 95 environmental conditions are calculated. The probability of structural components failures with the environmental condition within each interval are calculated by the interpolation method. The establishment of the database may be implemented through the following 3 steps:

Step1: Generating a set of input files with different combination of the environmental conditions. The environmental loads are extreme wind and wave loads caused by typhoons, which are assessed in Section 4.1.2. In the present example, 95 input files related to different environment loads $(V_{\mathrm{hub}}, H_{\mathrm{s}})$ are generated first, where the hub-height wind speed V_{hub} is assumed to change from 5 m/s – 100 m/s.

Step2: Running structural analysis and to assess the extreme response. Based on the generated input files, the structural analysis is implemented by running FAST. The turbulent wind (i.e., wind speed and wind direction) time histories are evaluated using the software package Turbsim [72]. Then FAST calculates the wind load on the blades using the Blade Element Momentum. The JONSWAP spectrum is used to model the wave spectrum and the inverse Fourier transform is applied to generate a wave-height time history. Then this time series is converted into structural loads by the FAST software package HydroDyn using Morrison's equation [73]. Based on the wave-height time history, the kinematics of individual water particles distributed along the monopile are calculated using the second order wave model [73,74]. The maximum bending moment of the tower and the maximum blade root flapwise moment can be identified from the output file where the time series of structural responses (i.e., bending moment of the tower and blade root flapwise moment) are recorded. More details for the simulations can be found from [19,21,75].

Step3: Calculating the probability of failure and formulate the database of probability of failures. The considered structural components are the towers and blades since the monopile and transition pieces were observed to always fail after the tower had reached a 100% probability of failure [21]. The ultimate limit state failure is considered to analyze the reliability of the structural components. For towers, local buckling failure is considered; that is, the maximum moment of the tower exceeds the cross-section bending capacity. Following Tarp-Johansen and Sørensen [76], the bending capacity of the tower can be calculated by:

$$M_{\mathrm{cr}} = \frac{1}{6}\left(1 - 0.84\frac{D}{t}\frac{F_{\mathrm{y}}}{E}\right)\left(D^3 - (D-2t)^3\right)F_{\mathrm{y}} \tag{20}$$

where D and t are the diameter and thickness of the tower, which are provided in Table 2; E and F_{y} are the Young's modulus and the yield strength for the steel, where the mean values are take from [70], and the coefficient of variation (CoV) is taken from [21,76]. The limit state function with consideration of uncertainties is expressed as:

$$G_{M_{\mathrm{cr}}} = M_{\mathrm{cr}}X_{\mathrm{mat}}X_{\mathrm{cr}} - M_{\mathrm{dem}}\left(H_{\mathrm{s}}, V_{hub}\right)X_{\mathrm{dyn}}X_{\mathrm{sim}}X_{\mathrm{str}} \tag{21}$$

where M_{dem} represents the maximum bending moment in each FAST simulation.

Similarly, the loading considered for the limit state of the blades is taken as the blade root flapwise moment capacity (M_{cap}) minus the flapwise moment demand (M_{dem}) [21] :

$$G_{\mathrm{bld}} = M_{\mathrm{cap}}X_{\mathrm{mat}}X_{\mathrm{cr}} - M_{\mathrm{dem}}\left(H_{\mathrm{s}}, V_{hub}\right)X_{\mathrm{dyn}}X_{\delta \mathrm{l}}X_{\mathrm{str}} \tag{22}$$

where the flapwise moment capacity M_{cap} is assumed to be 25740 kNm based on the calculation result of NREL 5 MW OWT blades designed by Resor [77]; M_{dem} is the maximum flapwise moment in each FAST simulation. More details on the mechanical characteristics and performances of wind turbine blades may be found from [77].

Table 4 provides the probabilistic models of uncertainties related to blade and tower failure modes, which stem form [21,76].

Table 4
Uncertainty model for blade and tower failure modes.

Type	Parameter	Mean	CoV	Distribution	Ref.
Model uncertainty	Structural dynamics (X_{dyn})	1	0.05	Lognormal	[21,76]
	Simulation statistics (X_{sim})	1	0.1	Normal	[21,76]
	Stress evaluation (X_{str})	1	0.03	Lognormal	[21,76]
	Blade model uncertainty ($X_{\delta 1}$)	1	0.05	Lognormal	[21,76]
	Critical load capacity (X_{cr})	1	0.10	Lognormal	[21,76]
	Material model uncertainty (X_{mat})	1	0.05	Lognormal	[21,76]
Material	Steel yield strength, Mpa (F_y)	240	0.05	Lognormal	[21,70,76]
	Steel Young's modulus (E)	2×10^5	0.25	Lognormal	[21,70,76]

Table 5
Failure rates for different considered components (/turbine/year).

Component	Failure_level 1	Failure_level 2	Failure_level 3
Gearbox	0.154	0.2772	0.4158
Hub	0.001	0.0018	0.0027
Generator	0.095	0.1710	0.2565
Circuit breaker	0.002	0.0036	0.0054
Pitch system	0.001	0.0018	0.0027
Yaw system	0.001	0.0018	0.0027
Controller	0.001	0.0018	0.0027
Transformer	0.001	0.0018	0.0027

4.2.2. Modeling of mechanical and electrical components failures

The performances of the considered components/subsystem listed in Table 5 are described by a homogeneous Poisson process (HPP) model [63], that is, the failure rate is constant with time. In Carroll [9], the failures are classified as a minor repair, major repair or major replacement according to the Reliawind categories [78], where the failure with a total repair material cost of less than €1000 is considered a minor repair, between €1000 and €10,000 a major repair and above €10,000 a major replacement. In this example, for simplicity, the major replacement associated with large losses and longer repair time is considered as the failure case, given that the conditional probability of resilience failure is assumed rather high for this classification. In order to study the effect of different reliability levels on resilience, three reliability levels are considered, see Table 5. The failure rates of level 1 is taken from the failure rates of the wind turbine components provided by Carroll [9], which are analyzed based on 350 offshore wind turbines of which the nominal power is between 2 and 4MW. This analysis defines a failure as a visit to a turbine, outside of a scheduled operation, at which material is consumed, which means that the considered failures could be various types of failures, such as fatigue failure. The failure rates of level 2 and 3 are assumed to be 1.8 and 2.7 times of level 1.

4.2.3. Modeling of cascading failures

Fig. 13 shows the cascading failure scenarios considered in the present example, including four major cascading failure scenarios:

- Blade strike. Many collapse cases of wind turbine tower are caused by the event that blade tip hits the tower due to huge deflection. If the blade fractures while the rotor revolves, it is likely to hit the tower shell which also may lead to tower collapse failure [79–81].
- Imbalance load. Another cause of OWT tower collapse failures, often seen in the past, concerns the imbalance of force generated by a blade failure [79].
- Cascading failure due to the failure of pitch and yaw systems. The pitch system can be used to start and stop the turbine by adjusting the angles of the blades in relation to the prevailing wind. The yaw system which serves to turn the nacelle around the tower axis can contribute to preventing the wind turbine from extreme loads in extreme wind conditions by rotating the wind turbine out of the wind. Therefore, these two systems play a vital role in regulating aerodynamic loads; by adjusting the blade pitch angle with changing wind speed and the nacelle yaw angle with changing wind direction [15,82,83].
- Tower collapse. The collapse of OWT towers may lead to a total loss of the OWT.

Table 6
Conditional failure probability of tower and blade (unit:/turbine/initial failure event).

Initial failed component	Blade	Tower
Pitch system	0.1	0.05
Yaw system	0.1	0.05
Blade	/	0.05

Table 7
Definition of the probabilistic model of T_{pre}.

Distribution	Preparedness level	Mean (Unit: hour)	CoV
Log-normal	Low	336	0.2
	High	168	

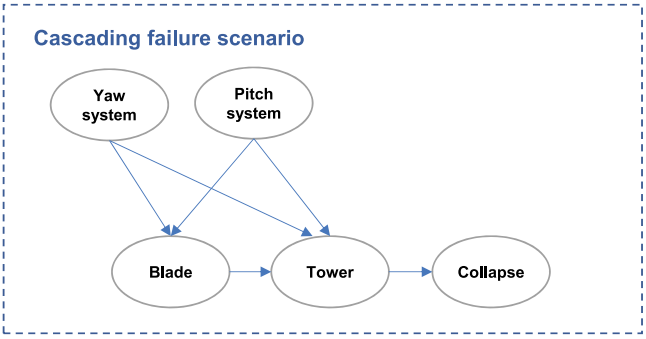

Fig. 13. Illustration of the cascading failure scenario considered in the present example.

It should be mentioned that, the failure rates of the components (i.e., electrical and mechanical components) listed in Table 5 already include cascading failures. This is because the causes of failure are not distinguished when the failure rate is counted here. Therefore, in the present example, only the scenarios which may lead to the cascading failures of blades and towers requires additional modeling. Since there are not sufficient reported cases about cascading failures, the probabilities of conditional failures are here simply given based on engineering judgement, see Table 6.

4.2.4. Modeling of failure consequences

The failure consequences are modeled according to Section 3.2.2. The maintenance costs associated with failure event can be calculated according to Eq. (7), where C_w is:

$$C_w = n_w \times c_w \times T_{rep} \tag{23}$$

where c_w is the cost for hiring 1 technician; $C_{material}$ is calculated by:

$$C_{material} = \sum_{i=1}^{n_c} C_i \tag{24}$$

Table 8
Repair time for different components (unit:hour), data is adapted from [9,22,86].

Distribution	Component	Mean (high preparedness)	Mean (low preparedness)	CoV
Log-normal	Gearbox	231	462	0.2
	Hub	298	596	
	Blade	288	576	
	Generator	81	162	
	Circuit breaker	150	300	
	Pitch	25	50	
	Yaw	49	98	
	Controller	12	24	
	Transformer	1	2	

Table 9
Material cost for different components (taken and adopted from [9] and [22]).

Component	Cost (USD)
Gearbox	725360
Hub	299600
Generator	189220
Circuit breaker	44152
Pitch	44152
Yaw	40998
Controller	40998
Transformer	497740
Blade	851510

Table 10
Labour and transportation cost.

Description	Cost (USD)
Labor cost/day (12 h)/technician	2027
Transportation cost/day	1399

where n_c is the number of the failed components, C_i is the material cost for the ith failed component; C_{trans} is calculated by:

$$C_{trans} = c_{trans} \times T_{rep} \tag{25}$$

where c_{trans} is the cost for transportation per time unit. T_{rep} is assumed to be calculated by:

$$T_{rep} = \frac{\sum_{i=1}^{n_c} T_i}{12 n_w} \tag{26}$$

where n_w is the number of technicians engaged in the repair work, which is assumed to be 4, 6, 8 for wind farms with 5, 10, 15 wind turbines; 12 represents that the technicians will work together for 12 h per day; n_c is the number of failed components; T_i is the repair time for the ith failed components, of which the probabilistic model can be found from Table 8. The strategy with respect to repair sequence is not considered in this example, and all events of failed wind turbines are assumed to have the same value of T_{rep}. The test period is considered only when the tower collapse happens, here T_{test} is assumed to be 3 months. The downtime can be calculated by Eq. (8), where the mean value of T_{pre} is assumed to be 7 days (168 h) and 14 days (336 h) for the high and low preparedness level respectively, see Table 7. Notice that the probabilistic model of T_{pre} in the present paper is rather simple, more details such as the modeling of the accessibility of the transportation to the wind turbine may be found from [84,85]. The CoV is assumed to be 0.2 according to the Refs. [9,22,86].

The parameters related with the cost model are adapted from [9], see Tables 9 and 10. In the event of tower collapse, it is assumed that the maintenance cost is 7,331,983 (USD).

4.3. Resilience quantification and sensitivity analysis for different decision alternatives

Based on the proposed resilience analysis and decision support framework in Section 3, in this section, the quantification of resilience of the OWFs addressed in the example are introduced and then a sensitivity analysis of the resilience performances of these is undertaken for the four categories of decision alternatives introduced in Section 4.1.1.

4.3.1. Resilience quantification

Monte Carlo (MC) simulations are applied to quantify the system resilience. According to Section 4.1.2, the random samples of V_{10} are generated. To simplify, the representation of the spatial dependency between the 10 min mean values of the wind velocity V_{10} at the locations of the different wind turbine a correlation coefficient ρ_I equal to 0.8 is assumed. Based on this assumption the corresponding random samples of V_{hub} and H_s are generated according to Eq. (13)–(17). As a next step, based on the probabilistic modeling and the reliability analysis presented in Section 4.2.1, the random samples of performances (failures/no failures) of structural components are generated. Meanwhile, the random samples of performances (failures/no failures) of mechanical and electrical components are generated according to the model introduced in Section 4.2.2. As outlined in Eq. (2), the economic capacity at the jth ($j = 1, 2, \ldots, T$) month is obtained by accumulating a fixed percentage χ of the benefits in the foregoing j-1 months:

$$R_r(j) = R_0 + \chi \sum_{i=1}^{n} \sum_{k=1}^{j-1} B_i(k) \tag{27}$$

where R_0 is the starting value of the economic capacity at the beginning of the service life, which in this example is assumed to be 5% of the expected value of the total service life benefits; n is the number of OWTs; T is the lifetime, which is set equal to 300 (months) in this example; $B_i(k)$ is the benefits of WT_i within the kth month calculated by Eq. (19). The economic demand $S_r(j)$ can be calculated following Eq. (3) and Eq. (23)–(25). Finally, the probability of resilience failure P_{RF} for different decision alternatives are calculated according to Eq. (4)–(5).

4.3.2. Sensitivity analysis for decision alternatives relevant to asset integrity management

In this section, the sensitivities of probability of resilience failure to the decision alternatives relevant to AIM as introduced in Section 4.1.1 are analyzed and the corresponding results are illustrated by Figs. 15–18, where Scenario 1–Scenario 6 represent the 6 reliability and preparedness decision scenarios, see Fig. 14. The failure rates and repair time of the 6 scenarios can be found from Table 5, Table 7, and Table 8.

Sensitivity analysis of χ. First of all, Fig. 15 shows the sensitivity of P_{RF} to changes in the percentage χ. It appears intuitive coherent that for increasing χ, P_{RF} is reducing. In addition, it is observed that the sensitivity of P_{RF} to changes in χ is growing over time. Further insights can be derived in support of decision-making, namely from Fig. 15 it is observed that if χ is too small, P_{RF} will be higher as time increases (e.g., when $\chi < 0.1$ in sub-figure (a), and when $\chi < 0.12$ in sub-figure (b)). This is caused by the effect of reserved benefits, i.e. the proportion of annual incomes reserved for building economic capacity, is not enough to support the maintenance costs. Therefore, the economic capacity of the system decreases over time and is eventually exhausted.

Table 7: Definition of the probabilistic model of T_{pr}

Distribution	Preparedness level	Mean (Unit: hour)	CoV
Log-normal	Low	336	0.2
	High	168	

Table 8: Repair time for different component

Distribution	Component	Mean (high preparedness)	Mean (low preparedness)	CoV
Log-normal	Gearbox	231	462	0.2
	Hub	298	596	
	Blade	288	576	
	Generator	81	162	
	Circuit breaker	150	300	
	Pitch	25	50	
	Yaw	49	98	
	Controller	12	24	
	Transformer	1	2	

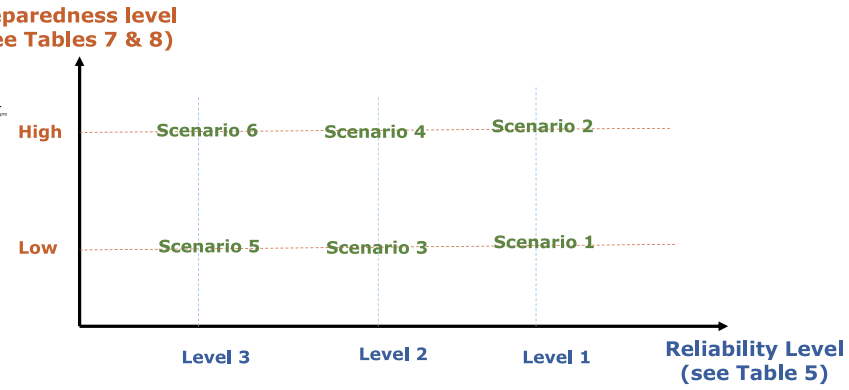

Table 5: Failure rates for different considered components (/turbine/year)

Component	Failure_Level 1	Failure_Level 2	Failure_Level 3
Gearbox	0.154	0.2772	0.4158
Hub	0.001	0.0018	0.0027
Generator	0.095	0.1710	0.2565
Circuit breaker	0.002	0.0036	0.0054
Pitch system	0.001	0.0018	0.0027
Yaw system	0.001	0.0018	0.0027
Controller	0.001	0.0018	0.0027
Transformer	0.001	0.0018	0.0027

Fig. 14. Reliability and preparedness decision scenarios.

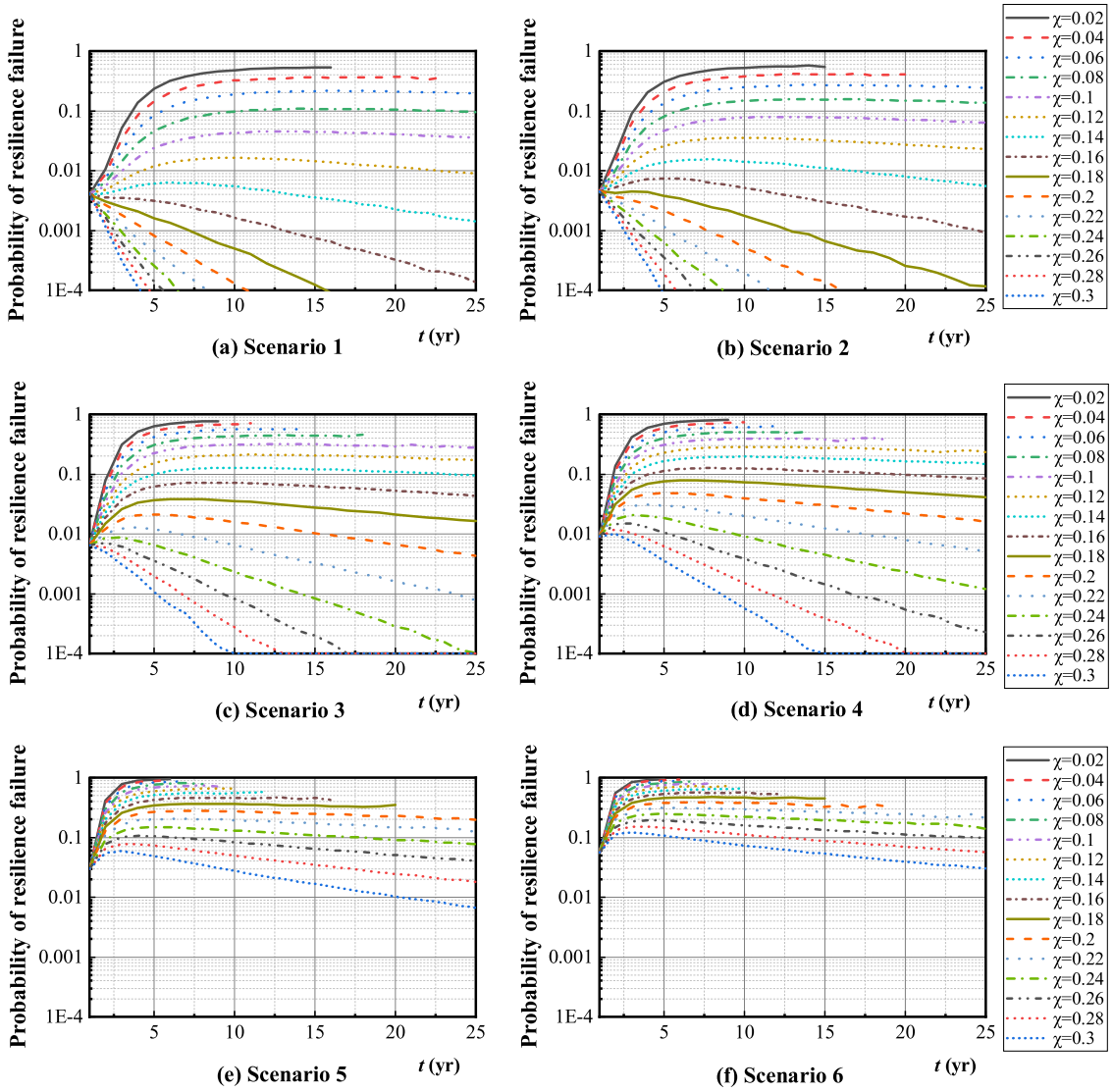

Fig. 15. Annual probability of resilience failure with the variation of the χ and time when n=10.

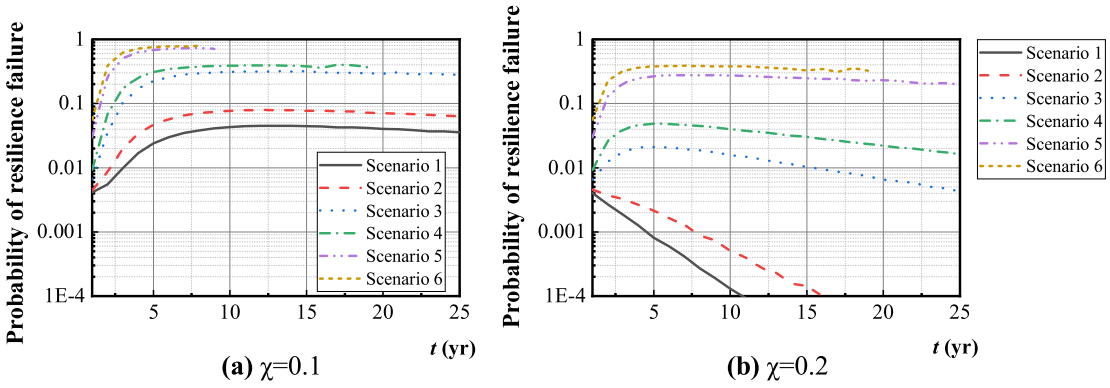

Fig. 16. Comparison of annual probability of resilience failure of as the function of t with different reliability and preparedness level.

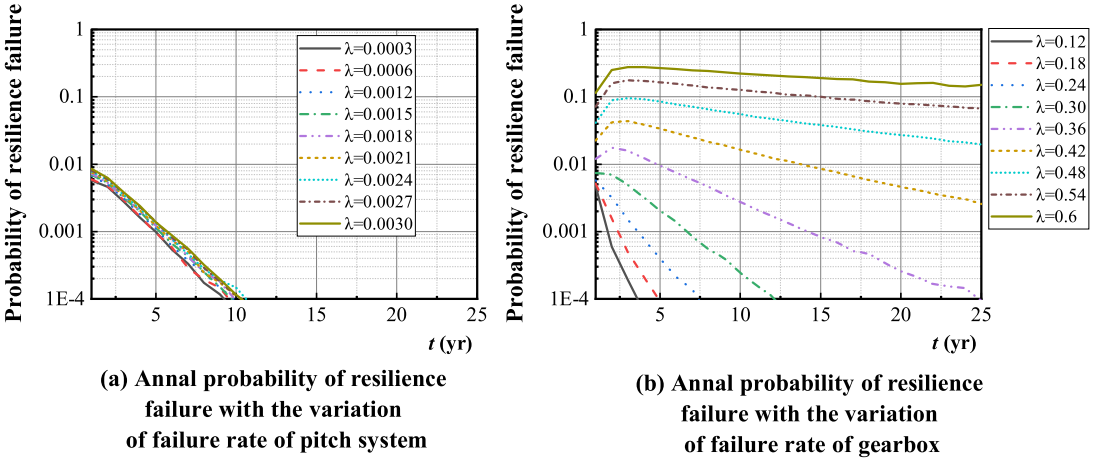

Fig. 17. Comparison of annual probability of resilience failure as the function of t with the variation of the pitch system and gearbox failure rates.

In such a condition, the P_{RF} at later years cannot be simulated. This is because when conducting MC simulations for the life-cycle simulation, most of the samples are failed in the earlier years due to the high P_{RF}, which leads to that there is no or less samples for the simulations in the later years. This problem may be solved by constantly increasing the number of MC simulations or some efficient sampling methods, but in actual decision-making, such high probability of resilience failure is almost non-existent, thus this is chosen to be ignored in the present work. In contrast, if χ is large, P_{RF} will decrease as a function of time (e.g., when $\chi \geq 0.1$ in sub-figure (a), and when $\chi \geq 0.12$ in sub-figure (b)) due to the increase of accumulated economic capacity. This implies that it is important to find a reasonable interval for χ, for which these effects are adequately balanced. By comparing the six sub-figures in Fig. 15 it is observed that the level of both the reliability and the preparedness can affect the width of this interval.

Sensitivity analysis of failure rates and repair time. Fig. 16 illustrates the sensitivity of P_{RF} to changes in the reliability and preparedness level under two different choices of χ. It can be observed by comparing sub-figure (a) and (b) that the influence of reliability and preparedness level is less pronounced in sub-figure (a), which indicates that P_{RF} is sensitive to the reliability level and the preparedness level when χ is high. This implies that it is not enough to improve resilience by increasing the level of reliability and preparedness, but also by improving the economic capacity. To further investigate the sensitivity of P_{RF} to the failure rates of components, Scenario 4 is chosen as basis, assuming that the failure rate (λ) of the pitch system varies from 0.0003 to 0.003 and the failure rate (λ) of the gearbox varies from 0.12 to 0.6, and the failure rates of other components remain constant. Fig. 17 shows the corresponding calculation results of P_{RF} with the variation of component failure rates. It is observed from both sub-figure (a) and (b) that P_{RF} is sensitive to the component failure rates, even for very small variations like the one in sub-figure (a). The effect on P_{RF} is more pronounced in sub-figure (b) due to the large variation in the failure rate of the gearbox. This may imply that choosing the more reliable gearbox is more effective in improving system resilience.

Sensitivity analysis of number of wind turbines. Finally, Fig. 18 compares the annual P_{RF} in year 5 for three OWFs composed of 5, 10, 15 OWTs, respectively. It can be observed from Fig. 18 that when P_{RF} is higher than a certain value, P_{RF} gradually increases as n increases. On the contrary, P_{RF} gradually decreases as n increases. It is noted that these values are all close to 0.1 in the four sub-figures. When P_{RF} is higher than this value, it implies that the economic capacity is not sufficient. In such situations, the OWFs with less OWTs are more resilient, since they are associated with smaller economic demands. When P_{RF} is lower than this value, the economic capacity is more adequate. In such situations, OWFs comprised of larger numbers of OWTs are more resilient, since the economic reserve generated by each individual OWT may be shared with others. It can be observed from sub-figure (a) that when P_{RF} is equal to 0.01, the OWF with 15 OWTs requires about 21% of the annual incomes reserved for building economic capacity, while for the OWF with 10 OWTs and 5 OWT's only about 22.5% and 26% are required to achieve the same level of resilience performance. For the purpose of resilience informed decision-making, if the decision alternatives concern OWF design alternatives (e.g., number of wind turbines in this figure), and if the maximum acceptable P_{RF} is lower than this value (0.1 in the present example), the OWF which has more OWTs should be chosen. The sensitivity analyses performed in the present study are undertaken at only at principal levels. More studies in the

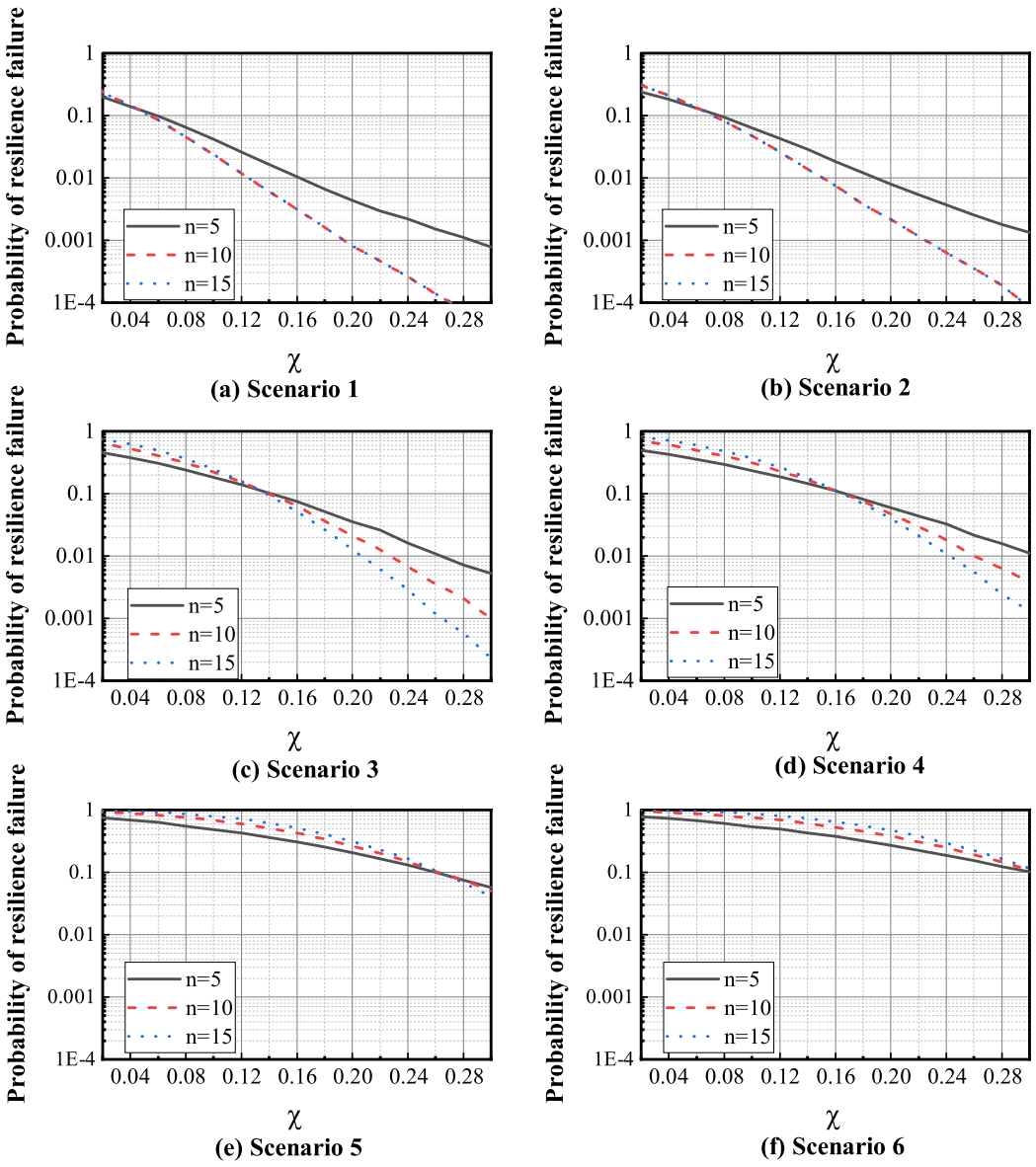

Fig. 18. Comparison of annual probability of resilience failure as the function of χ with different number of OWTs.

future, considering specific decision problems and addressing also the effect of the different prevailing uncertainties on these, would still be very relevant.

5. Conclusions

This paper develops a general probabilistic framework for resilience modeling and analysis of offshore wind farm (OWF), and illustrates how such a framework may be implemented within the modeling techniques and tools commonly applied in the industry. Based on the system representation of OWFs, resilience is modeled and quantified as a life-cycle performance, which accounts for not only the long-term environmental conditions and physical performance of OWF systems, but also the performance/capacity of the management and economic system which is related to the reorganization ability and the life-cycle benefits. In this way, the proposed framework facilitates the optimization of decisions on AIM from a life-cycle perspective. Based on the proposed framework, acceptable and optimal decisions may be identified by quantifying the life-cycle resilience performance of the OWFs under different AIM decision alternatives.

The application illustrates the relationship between resilience performance and different decision alternatives. The key findings of the case study can be summarized as follows: (i) except for the reliability level which is normally chosen as a design alternative, the preparedness level, which represents the ability of the management system, is also a key factor affecting the resilience of OWFs; (ii) the effects of reliability level and preparedness level are not significant when the economic capacity is low, which emphasizes the importance of the optimization of the economic capacity (by optimizing χ in the present framework) in the optimal decision-making of OWFs; (iii) when the economic capacity is enough, OWFs comprised of larger numbers of OWTs are more resilient, while when the economic capacity is insufficient, OWFs comprised of smaller numbers of OWT's are more resilient. The *LCoE* of the OWF with different decision alternatives is not calculated in the present example, however, it should be noted that even though the OWF with high reliability and preparedness levels may perform better in terms of resilience, these decisions may lead to higher initial investment resulting in higher *LCoE*, as introduced in Section 3.3.

For illustration purposes, the application in the present paper still includes simplifications with potentials for improvements. But the framework proposed in the present paper may have many applications

for different aspects of integrity management. Further research may be directed on the integration of deterioration and fatigue failure of OWT components and explicit address of structural health monitoring and inspections into the optimization of OWF resilience characteristics. Further research should also aim to refine the modeling of the recovery process, so that the repair costs and repair time may be estimated more accurately. The study of the application also shows that the choice concerning the allocation of economic resources represented by χ, is crucial for resilience management. Further research should investigate the trade-off between the economic reserve supporting the recovery cost and the net benefit representing the competitiveness of an OWF project.

CRediT authorship contribution statement

Min Liu: Conceptualization, Methodology, Software, Writing – original draft. **Jianjun Qin:** Methodology, Writing – review & editing. **Da-Gang Lu:** Conceptualization, Supervision, Writing – review & editing. **Wei-Heng Zhang:** Methodology. **Jiang-Sheng Zhu:** Resources. **Michael Havbro Faber:** Conceptualization, Supervision, Writing – review & editing.

Declaration of competing interest

The authors declare that they have no known competing financial interests or personal relationships that could have appeared to influence the work reported in this paper.

Acknowledgments

This work is jointly supported by the National Key Research and Development Plan of China "Basic Theory and Methods for Resilience Assessment and Risk Control of Transportation Infrastructures" (Grant No. 2021YFB2600500).

The authors express our deepest gratitude to the editors and anonymous reviewers, whose careful work and thoughtful suggestions have helped to improve this paper considerably.

References

[1] Leung DY, Yang Y. Wind energy development and its environmental impact: A review. Renew Sustain Energy Rev 2012;16(1):1031–9.
[2] Costoya X, DeCastro M, Carvalho D, Gómez-Gesteira M. On the suitability of offshore wind energy resource in the United States of America for the 21st century. Appl Energy 2020;262:114537.
[3] Fattahi A, Sijm J, Faaij A, et al. Modelling a highly decarbonised North sea energy system in 2050: A multinational approach. Adv Appl Energy 2021;100080.
[4] McKenna R, D'Andrea M, González MG. Analysing long-term opportunities for offshore energy system integration in the Danish north sea. Adv Appl Energy 2021;4:100067.
[5] Zhao N, You F. New york state's 100% renewable electricity transition planning under uncertainty using a data-driven multistage adaptive robust optimization approach with machine-learning. Adv Appl Energy 2021;2:100019.
[6] Global Wind Energy Council. Global offshore wind report 2020. Tech. rep., Global Wind Energy Council: Brussels, Belgium; 2020.
[7] Ribrant J, Bertling LM. Survey of failures in wind power systems with focus on Swedish wind power plants during 1997–2005. IEEE Trans Energy Convers 2007;22(1):167–73.
[8] Gayo JB. Reliability–focused research on optimizing Wind Energy system design, operation and maintenance: Tools, proof of concepts, guidelines & methodologies for a new generation. Tech. rep., Gamesa Innovation and Technology: Egues, Spain; 2011.
[9] Carroll J, McDonald A, McMillan D. Failure rate, repair time and unscheduled O&M cost analysis of offshore wind turbines. Wind Energy 2016;19(6):1107–19.
[10] Artigao E, Martín-Martínez S, Honrubia-Escribano A, Gómez-Lázaro E. Wind turbine reliability: A comprehensive review towards effective condition monitoring development. Appl Energy 2018;228:1569–83.
[11] Ioannou A, Angus A, Brennan F. A lifecycle techno-economic model of offshore wind energy for different entry and exit instances. Appl Energy 2018;221:406–24.
[12] Scheu MN, Kolios A, Fischer T, Brennan F. Influence of statistical uncertainty of component reliability estimations on offshore wind farm availability. Reliab Eng Syst Saf 2017;168:28–39.
[13] Kang J, Soares CG. An opportunistic maintenance policy for offshore wind farms. Ocean Eng 2020;216:108075.
[14] Rinaldi G, Garcia-Teruel A, Jeffrey H, Thies PR, Johanning L. Incorporating stochastic operation and maintenance models into the techno-economic analysis of floating offshore wind farms. Appl Energy 2021;301:117420.
[15] Kim M-G, Dalhoff PH. Yaw systems for wind turbines – Overview of concepts, current challenges and design methods. J Phys Conf Ser 2014;524(1):012086.
[16] Young IR. Parametric hurricane wave prediction model. J Waterw Port Coast Ocean Eng 1988;114(5):637–52.
[17] Li D, Geyer B, Bisling P. A model-based climatology analysis of wind power resources at 100-m height over the Bohai sea and the Yellow sea. Appl Energy 2016;179:575–89.
[18] Hong L, Möller B. Risks of tropical cyclones on offshore wind farms in China. In: 6th Dubrovnik conference on sustainable development of energy, water and environment systems. 2011.
[19] Hallowell ST. A framework to assess hurricane risk to offshore wind turbines including breaking waves (Ph.D. thesis), Northeastern University; 2016.
[20] Hallowell ST, Myers AT, Arwade SR, Pang W, Rawal P, Hines EM, et al. Hurricane risk assessment of offshore wind turbines. Renew Energy 2018;125:234–49.
[21] Wilkie D, Galasso C. A probabilistic framework for offshore wind turbine loss assessment. Renew Energy 2020;147:1772–83.
[22] Ambühl S, Sørensen JD. Different transportation and maintenance strategies for offshore wind farms. Tech. rep, Department of Civil Engineering, Aalborg University; 2017.
[23] Jonker T. The development of maintenance strategies of offshore wind farm. 2017, Literature Assignment ME54010.
[24] Lin Z, Cevasco D, Collu M. A methodology to develop reduced-order models to support the operation and maintenance of offshore wind turbines. Appl Energy 2020;259:114228.
[25] Zhang W-H, Qin J, Lu D-G, Thöns S, Faber MH. Voi-informed decision-making for SHM system arrangement. Struct Health Monit 2020;1475921720962736.
[26] Maienza C, Avossa A, Ricciardelli F, Coiro D, Troise G, Georgakis CT. A life cycle cost model for floating offshore wind farms. Appl Energy 2020;266:114716.
[27] Pimm SL. The complexity and stability of ecosystems. Nature 1984;307(5949):321–6.
[28] Holling CS. Engineering resilience versus ecological resilience. Eng Ecol Constrain 1996;31(1996):32.
[29] Shittu E, Tibrewala A, Kalla S, Wang X. Meta-analysis of the strategies for self-healing and resilience in power systems. Adv Appl Energy 2021;100036.
[30] Marqusee J, Becker W, Ericson S. Resilience and economics of microgrids with PV, battery storage, and networked diesel generators. Adv Appl Energy 2021;100049.
[31] Bruneau M, Chang SE, Eguchi RT, Lee GC, O'Rourke TD, Reinhorn AM, et al. A framework to quantitatively assess and enhance the seismic resilience of communities. Earthq Spectra 2003;19(4):733–52.
[32] Zhou Y, Panteli M, Moreno R, Mancarella P. System-level assessment of reliability and resilience provision from microgrids. Appl Energy 2018;230:374–92.
[33] Roege PE, Collier ZA, Mancillas J, McDonagh JA, Linkov I. Metrics for energy resilience. Energy Policy 2014;72:249–56.
[34] Moslehi S, Reddy TA. Sustainability of integrated energy systems: A performance-based resilience assessment methodology. Appl Energy 2018;228:487–98.
[35] Faber MH, Qin J, Miraglia S, Thöns S. On the probabilistic characterization of robustness and resilience. Procedia Eng 2017;198:1070–83.
[36] Faber MH, Miraglia S, Qin J, Stewart MG. Bridging resilience and sustainability-decision analysis for design and management of infrastructure systems. Sustain Resil Infrastruct 2018;5(1–2):102–24.
[37] Ouyang M, Dueñas-Osorio L, Min X. A three-stage resilience analysis framework for urban infrastructure systems. Struct Saf 2012;36:23–31.
[38] Sharma N, Tabandeh A, Gardoni P. Regional resilience analysis: A multiscale approach to optimize the resilience of interdependent infrastructure. Comput-Aided Civ Infrastruct Eng 2020;35(12):1315–30.
[39] Bao M, Ding Y, Sang M, Li D, Shao C, Yan J. Modeling and evaluating nodal resilience of multi-energy systems under windstorms. Appl Energy 2020;270:115136.
[40] Chou J-S, Chiu C-K, Huang I-K, Chi K-N. Failure analysis of wind turbine blade under critical wind loads. Eng Fail Anal 2013;27:99–118.
[41] Chen X, Li C, Tang J. Structural integrity of wind turbines impacted by tropical cyclones: A case study from China. J Phys Conf Ser 2016;753(4):042003.
[42] Xiao Y. Typhoon wind hazard analysis based on numerical simulation and fragility of light-gauge steel structure in southeast China coastal regions (Ph.D. thesis), Harbin Institute of Technology, Harbin; 2011.
[43] Zhang S. Assessment of typhoon induced wind risk under climate change in Japan (Ph.D. thesis), ETH Zurich; 2013.
[44] Jayaram N, Baker J. Probabilistic seismic lifeline risk assessment using efficient sampling and data reduction techniques (Ph.D. thesis), Stanford University, Stanford; 2010.

[45] Li Y, Dong Y, Qian J. Higher-order analysis of probabilistic long-term loss under nonstationary hazards. Reliab Eng Syst Saf 2020;107092.
[46] Mardfekri M, Gardoni P. Multi-hazard reliability assessment of offshore wind turbines. Wind Energy 2015;18(8):1433–50.
[47] Bazilevs Y, Deng X, Korobenko A, Lanza di Scalea F, Todd M, Taylor S. Isogeometric fatigue damage prediction in large-scale composite structures driven by dynamic sensor data. J Appl Mech 2015;82(9).
[48] Bazilevs Y, Korobenko A, Deng X, Yan J. Fluid–structure interaction modeling for fatigue-damage prediction in full-scale wind-turbine blades. J Appl Mech 2016;83(6).
[49] Muñoz GR, Sørensen JD. Probabilistic inspection planning of offshore welds subject to the transition from protected to corrosive environment. Reliab Eng Syst Saf 2020;202:107009.
[50] Ditlevsen O. Stochastic model for joint wave and wind loads on offshore structures. Struct Saf 2002;24(2–4):139–63.
[51] Alexiadis M, Dokopoulos P, Sahsamanoglou H. Wind speed and power forecasting based on spatial correlation models. IEEE Trans Energy Convers 1999;14(3):836–42.
[52] Lei M, Shiyan L, Chuanwen J, Hongling L, Yan Z. A review on the forecasting of wind speed and generated power. Renew Sustain Energy Rev 2009;13(4):915–20.
[53] Kusiak A, Song Z. Design of wind farm layout for maximum wind energy capture. Renew Energy 2010;35(3):685–94.
[54] Zhou W, Yang H, Fang Z. Wind power potential and characteristic analysis of the Pearl River Delta region, China. Renew Energy 2006;31(6):739–53.
[55] Ozay C, Celiktas MS. Statistical analysis of wind speed using two parameter Weibull distribution in Alaçati region. Energy Convers Manage 2016;121:49–54.
[56] Lepore A, Palumbo B, Pievatolo A. A Bayesian approach for site-specific wind rose prediction. Renew Energy 2020;150:691–702.
[57] Loukatou A, Howell S, Johnson P, Duck P. Stochastic wind speed modelling for estimation of expected wind power output. Appl Energy 2018;228:1328–40.
[58] Qin J. Improved probabilistic modeling of wind speed in the context of structural risk assessment. KSCE J Civ Eng 2018;22(3):896–902.
[59] Qin J, Faber MH. Resilience informed integrity management of wind turbine parks. Energies 2019;12(14):2729.
[60] on Structural Safety JC. Risk assessment in engineering. Principles, system representation and risk criteria. 2008, ETH Zurich.
[61] Sørensen JD, Toft HS. Probabilistic design of wind turbines. Energies 2010;3(2):241–57.
[62] Toft HS, Sørensen JD. Reliability-based design of wind turbine blades. Struct Saf 2011;33(6):333–42.
[63] Tavner PJ, Xiang J, Spinato F. Reliability analysis for wind turbines. Wind Energy Int J Prog Appl Wind Power Convers Technol 2007;10(1):1–18.
[64] Ozturk S, Fthenakis V, Faulstich S. Failure modes, effects and criticality analysis for wind turbines considering climatic regions and comparing geared and direct drive wind turbines. Energies 2018;11(9):2317.
[65] Glavind ST, Sepulveda JG, Faber MH. On a simple scheme for systems modeling and identification using big data techniques. Reliab Eng Syst Saf 2021;108219.
[66] Asgarpour M. Risk and reliability based O&M planning of offshore wind farms (Ph.D. thesis), Aalborg University; 2018.
[67] of Shipping AB. Guide for building and classing floating offshore wind turbine installations. American Bureau of Shipping Houston, TX, USA; 2013.
[68] Kaltschmitt M, Streicher W, Wiese A. Renewable energy: technology, economics and environment. Springer Science & Business Media; 2007.
[69] IEC 61400-3-1:2019. Wind energy generation systems-part 3-1: Design requirements for fixed offshore wind turbines. 2019, International Electrotechnical Commission.
[70] Jonkman J, Butterfield S, Musial W, Scott G. Definition of a 5-MW reference wind turbine for offshore system development. Tech. rep, National Renewable Energy Lab.(NREL), Golden, CO (United States); 2009.
[71] Jonkman B, Jonkman J. FAST v8. 16.00 a-bjj. Tech. rep., National Renewable Energy Lab.(NREL), Golden, CO (United States); 2016.
[72] Kelley ND, Jonkman BJ. Overview of the turbsim stochastic inflow turbulence simulator: Version 1.21. Tech. rep., National Renewable Energy Lab.(NREL), Golden, CO (United States); 2007.
[73] Jonkman JM, Robertson A, Hayman GJ. HydroDyn user's guide and theory manual. Tech. rep., National Renewable Energy Lab.(NREL), Golden, CO (United States); 2014.
[74] Bredmose H, Mariegaard J, Paulsen BT, Jensen B, Schløer S, Larsen TJ, et al. The wave loads project. DTU Wind Energy, Denmark; 2013.
[75] Morató A, Sriramula S, Krishnan N, Nichols J. Ultimate loads and response analysis of a monopile supported offshore wind turbine using fully coupled simulation. Renew Energy 2017;101:126–43.
[76] Tarp-Johansen N, Sørensen JD, Madsen PH. Experience with acceptance criteria for offshore wind turbines in extreme loading. In: Workshop on reliability based code calibration. 2002.
[77] Resor BR. Definition of a 5MW/61.5 m wind turbine blade reference model. Albuquerque, New Mexico, USA, Sandia National Laboratories, SAND2013-2569; 2013.
[78] GH ReliaWind. Reliability focused research on optimizing wind energy systems design, operation and maintenance: tools, proof of concepts, guidelines & methodologies for a new generation. 2007, Reliawind, Rep.
[79] Ma Y, Martinez-Vazquez P, Baniotopoulos C. Wind turbine tower collapse cases: A historical overview. Proc Inst Civ Eng-Struct Build 2019;172(8):547–55.
[80] Deng Y, Xie T, Zhang G, Lei H, Tian d. Blade tip deflection calculations and safety analysis of wind turbine. In: IET conference proceedings. Institution of Engineering and Technology; 2013.
[81] Brouwer SR, Al-Jibouri SH, Cárdenas IC, Halman JI. Towards analysing risks to public safety from wind turbines. Reliab Eng Syst Saf 2018;180:77–87.
[82] Kim E, Manuel L. Hurricane-induced loads on offshore wind turbines with considerations for nacelle yaw and blade pitch control. Wind Eng 2014;38(4):413–23.
[83] Bharatbhai MG. Failure mode and effect analysis of repower 5M wind turbine. Int J Adv Res Eng Sci Technol 2015;2(5).
[84] Lazaridis L. Economic comparison of HVAC and HVDCSolutions for large offshore wind farms underspecial consideration of reliability. 2005.
[85] Ambühl S, Dalsgaard Sørensen J. Sensitivity of risk-based maintenance planning of offshore wind turbine farms. Energies 2017;10(4):505.
[86] Ambühl S, Marquis L, Kofoed JP, Sørensen JD. Operation and maintenance strategies for wave energy converters. Proc Inst Mech Eng O 2015;229(5):417–41.